

# Lattice QCD - A guide for people who want results

**Christine Davies**

Department of Physics and Astronomy,  
University of Glasgow, UK

arXiv:hep-lat/0509046v1 15 Sep 2005

## 1 Introduction

Lattice QCD was invented thirty years ago but only in the last few years has it finally fulfilled its promise as a precision tool for calculations in hadron physics. This review will cover the fundamentals of discretising QCD onto a space-time lattice and how to reduce the errors associated with the discretisation. This ‘improvement’ is the key that has made the enormous computational task of a lattice QCD calculation tractable and enabled us to reach the recent milestone of precision calculations of simple ‘gold-plated’ hadron masses. Accurate decay matrix elements, such as those for leptonic and semileptonic decay of heavy mesons needed by the  $B$  factory experimental programme, are now within sight. I will describe what goes into such calculations and what the future prospects and limitations are.

## 2 Lattice QCD formalism and methods

### 2.1 The Path Integral

Lattice QCD is based on the path integral formalism. We can demonstrate this formalism by discussing the solution of the quantum mechanical problem of a particle moving in one dimension (Lepage 1998a). This could be solved using Schrödinger’s equation with  $H = p^2/2m + V(x)$  and  $[x, p] = i$  (in ‘particle physics units’,  $\hbar = c = 1$ ). We can also solve it using the path integral formulation and this is the basis for lattice QCD.

A key quantity is the transition amplitude between eigenstates of position at, say, time  $t = t_i$  and  $t_f$ . This is expressed as a functional integral over all possible paths  $x(t)$

from  $t = t_i$  to  $t_f$  weighted by the exponential of the action,  $S$ , which is the integral of the Lagrangian,  $L$ .

$$\langle x_f(t_f) | x_i(t_i) \rangle = \int \mathcal{D}x(t) e^{iS[x]} \quad (1)$$

$$S[x] \equiv \int_{t_i}^{t_f} dt L(x, \dot{x}) \equiv \int dt \left[ \frac{m\dot{x}(t)^2}{2} - V(x(t)) \right]. \quad (2)$$

The path integral can be evaluated by discretising time into a set of points,  $t_j = t_i + ja$  for  $j = 0, 1 \dots N$  and  $a$  the lattice spacing  $\equiv (t_f - t_i)/N$ . The path  $x(t)$  then becomes a set of variables,  $x_j$ , and Equation 1 above requires us to integrate over each one, *ie* the problem reduces to an ordinary integral but over an  $N - 1$ -dimensional space. The end points,  $x_0$  and  $x_N$  are kept fixed in this example. The most likely path is the classical one, which minimises the action ( $m\ddot{x} = V'$ ), but the path integral allows quantum fluctuations about this, see Figure 1.

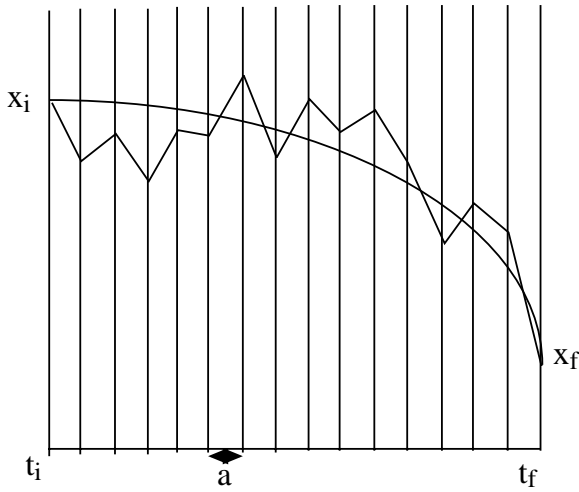


**Figure 1.** Discretised classical and possible quantum mechanical paths from  $x_i$  to  $x_f$  for a particle moving in one dimension.

The  $i$  in front of the action in the exponential gives rise to the problem, both conceptual and numerical, of adding oscillating quantities together. It is simpler to rotate the time axis to Euclidean time,  $t \rightarrow -it$ . Then the path integral becomes

$$\int \mathcal{D}x(t) e^{-S[x]} = A \int_{-\infty}^{\infty} dx_1 dx_2 \dots dx_{N-1} e^{-S[x]} \quad (3)$$

$$S[x] \equiv \int_{t_i}^{t_f} L(x, \dot{x}) \equiv \sum_{j=0}^{N-1} \left[ \frac{m\dot{x}_j^2}{2} + V(x_j) \right],$$

where the integrals over the intermediate points in the path,  $x(t)$ , are now explicit. We will ignore the normalisation of the integral,  $A$ . To perform the integral we must discre-

tise the Lagrangian so that it takes values at the discrete time points. Then

$$S = \sum_{j=0}^{N-1} \left[ \frac{m}{2a} (x_{j+1} - x_j)^2 + aV(x_j) \right]. \quad (4)$$

Clearly the accuracy of our discretisation will depend on  $a$  being small. However, as  $a$  becomes smaller at fixed physical time length, the number of points,  $N$ , increases and so does the computational cost.

For large  $N$  an efficient way to perform the integral is by Monte Carlo. A set of possible values for  $x_j$ ,  $j = 1, N$  is called a *configuration*. The configurations with most weight in the integral are those with large  $e^{-S}$ . For maximum efficiency we want to generate configurations with probability  $e^{-S}$  - this is known as *importance sampling*. A simple method for doing this is the Metropolis algorithm. This starts with an initial configuration (eg  $x_j$  all zero or chosen randomly). It then passes through the  $x_j$  in turn proposing a change to a given  $x_k$  of size  $\epsilon$ , ie a random number between  $-\epsilon$  and  $\epsilon$  temporarily added to  $x_k$ , say. The change in the action as a result of  $x_k$  changing is calculated. Call this  $\Delta S$ . Note that this calculation only involves the  $x_j$  in the neighbourhood of  $x_k$  and connected to it through the action. If  $\Delta S < 0$  the change is accepted. If  $\Delta S > 0$  another random number, uniformly distributed between 0 and 1 is generated. If  $e^{-\Delta S} > rand$  then the change is accepted. If not,  $x_k$  reverts to its previous value. (Lepage 1998a, di Pierro 2000)

In this way a new configuration is generated after each sweep through the lattice. A set of configurations is called an *ensemble*. Calculations of various functions of the  $x_j$  on an ensemble then yield the physics results that we are after, such as the quantised energy levels available to the particle.

In wavefunction language we can express

$$\langle x_f | e^{-iH(t_f - t_i)} | x_i \rangle = \sum_n \psi_n^*(x_f) \psi_n(x_i) e^{-iE_n(t_f - t_i)}, \quad (5)$$

by inserting a complete set of eigenstates of the Hamiltonian,  $H$ . When rotated to Euclidean time, and taking  $t_f - t_i = T$  and  $x_i = x_f = x$  we have

$$\langle x | e^{-HT} | x \rangle = \sum_n \psi_n^*(x) \psi_n(x) e^{-E_n T}, \quad (6)$$

where  $\psi_n(x) = \langle n | x \rangle$ . It now becomes clear that the result will be dominated by the ground state as  $T$  becomes large, because all higher states are exponentially suppressed. Integrating over the initial and final  $x$  values gives:

$$\int dx \langle x | e^{-HT} | x \rangle \rightarrow e^{-E_0 T}, T \rightarrow \infty. \quad (7)$$

This would be the result, up to a normalisation, of integrating by Monte Carlo over all the  $x_j$ , setting the initial and final values to be the same, ie using periodic boundary conditions. The result looks very similar to a problem in statistical mechanics when formulated in this way, as did Equation 3, and this is not an accident. Indeed we can work at non-zero temperature if we take  $T$  finite, but here we will concentrate on the zero temperature case where in principle  $T \rightarrow \infty$ , and in practice is large.

To investigate excitations above the ground state, we must interrupt the propagation of the ground state by introducing new operators at intermediate times. For example,

$$\begin{aligned} \frac{\langle x(T)|x(t_2)x(t_1)|x(0)\rangle}{\langle x(T)|x(0)\rangle} &= \frac{\int \mathcal{D}x \ x(t_2)x(t_1)e^{-S[x]}}{\int \mathcal{D}x \ e^{-S[x]}} \\ &= |\langle E_0|x|E_1\rangle|^2 e^{-(E_1-E_0)(t_2-t_1)}, t_2 - t_1 \rightarrow \infty. \quad (8) \end{aligned}$$

The state propagating between the insertions of the  $x$  operators at  $t_1$  and  $t_2$  cannot be the ground state, since  $x$  switches parity. If  $t_2 - t_1$  is large enough then the first excited state will dominate, by the same argument as used above for ground state domination. So, if we can evaluate the ratio of path integrals, we can determine the energy splitting  $E_1 - E_0$  between the first excited and the ground state. The evaluation is very simply done by taking an ensemble of configurations generated by the Metropolis algorithm above and ‘measuring’ on each one the value of  $x(t_2)x(t_1)$ . The ensemble average of this quantity, denoted  $\langle\langle x(t_2)x(t_1) \rangle\rangle$ , is then the ratio above.

The evaluation will suffer from a statistical error depending on how many configurations are in the ensemble. This will improve as the square root of the number of configurations provided that the results on each configuration are statistically independent. Since the configurations were made in a sequence, this will not be strictly true and results on neighbouring configurations in the sequence will be correlated. There are various statistical techniques, such as binning (averaging) neighbouring results and then recalculating the statistical error, that will uncover correlations. If the statistical error grows with the bin size then the results are correlated and the binned results should be used rather than the raw results. It might also be true that results on some number of the initial configurations of an ensemble have to be discarded because these configurations, and measurements on them, are not yet typical of the  $e^{-S}$  distribution. For this example, the results can obviously be improved statistically by moving  $t_1$  and  $t_2$  along the time axis, keeping  $t_2 - t_1$  fixed, and averaging those results.

To extract  $E_1 - E_0$  we should fit the results as a function of  $t_2 - t_1$  to the exponential form of Equation 8. Since  $t_2 - t_1$  will not be infinite, we can take account of contamination from higher states by fitting to a sum of exponentials in which we constrain the higher  $E_n > E_1$ . Finally we may also improve the accuracy on the energy by modifying the operator  $x(t_1)x(t_2)$  to a product of functions of  $x(t_{1,2})$  which has optimum overlap with the first excited state and minimum overlap with higher excited states. This will allow Equation 8 to become true for smaller values of  $t_2 - t_1$  and improve the extraction of  $E_1 - E_0$  from the fits. Indeed we can fit simultaneously to the results from several different operators and this again will improve the accuracy with which  $E_1 - E_0$  can be determined. It is a useful exercise to do the calculation above for, say, the simple harmonic oscillator potential,  $V = x^2/2$  and  $m = 1$ . All the pitfalls of ‘measurement’ and the improvements above have their mirror in lattice QCD calculations, as we shall see, but this simple example demonstrates them very clearly in a setting where computer time is not an issue.

An important issue is that of the systematic errors, called discretisation errors, introduced because of the non-zero lattice spacing. We can make these explicit by rewriting the finite difference in terms of the continuum (*ie* continuous space-time of the real world) derivative. The exponential of the continuum derivative is the translation operator

for moving from one site to the next. So

$$\frac{x_{i+1} - x_i}{a} = \frac{e^{\partial a} - 1}{a} = \partial + \frac{a\partial^2}{2}. \quad (9)$$

This shows that this form of the finite difference has errors linear in  $a$ . The actual size of the errors at a given value of  $a$  would depend on the effective size of  $\partial^2$  in the quantity being calculated. To halve the errors requires half the lattice spacing at (at least) double the computer cost.

The situation is significantly improved by using an improved discretisation.  $\Delta x_i = (x_{i+1} - x_{i-1})/2a$  has errors first at  $\mathcal{O}(a^2)$ . Further improvement is obtained by correcting for the  $a^2$  error using

$$\Delta x_i - \frac{a^2}{6}(\Delta)^3 x_i \quad (10)$$

where  $(\Delta)^3$  is a discretisation of the third order derivative. Errors are then  $\mathcal{O}(a^4)$  and this means very much smaller errors at a given value of  $a$ , or a huge reduction in computer cost for a given error by being able to work at a larger value of  $a$ . The improved discretisation costs a little in computer power to implement but this is completely negligible compared to the computer cost saving of the improvement and it is this that has made lattice QCD calculations tractable.

## 2.2 Gluon fields in lattice QCD

Now we have all the ingredients for lattice QCD. The position operator as a function of time is replaced by the quark and gluon field operators as a function of four-dimensional space-time. We discretise the space-time into a lattice of points (Figure 2) in order to be able to calculate the Feynman Path Integral numerically, using Monte Carlo methods on a computer. The ground-state which dominates the path integral is the QCD vacuum and we will be interested in excitations of this which correspond to hadrons.

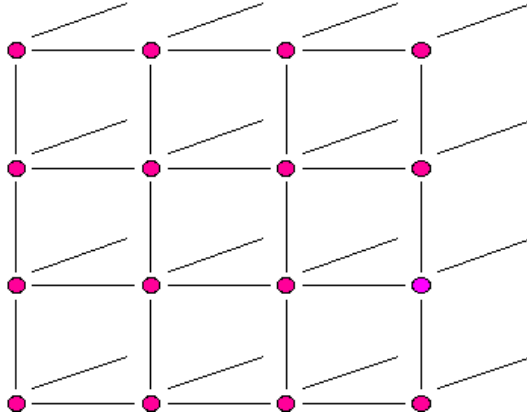


**Figure 2.** A 2-dimensional rendition of a 3-dimensional cubic lattice. Lattice QCD calculations use a 4-dimensional grid.

It is important to remember that lattice QCD is not complicated. It is a straightforward simulation of the theory on a computer, but a numerically intensive one. It is the theory of QCD that is being simulated, not a model. However, we are limited in the things that we can calculate. There are also statistical and systematic errors associated with the calculations and it is important to understand where they come from, so that you can assess the usefulness of a particular calculation for your needs.

Consider the operator  $\mathcal{O} = (\bar{\psi}\psi)_y(\bar{\psi}\psi)_x$ . This creates a hadron at a point  $x$  and destroys it at a point  $y$ . This is the QCD generalisation of the  $x(t_1)x(t_2)$  operator of the previous section. Then the matrix element in the vacuum of the operator is given in path integral form as:

$$\langle 0|\mathcal{O}|0\rangle = \frac{\int [d\psi] [d\bar{\psi}] [dA_\mu] \mathcal{O}[\psi, \bar{\psi}, A] e^{-S}}{\int [d\psi] [d\bar{\psi}] [dA_\mu] e^{-S_{QCD}}}. \quad (11)$$

The path integral runs over all values of the quark and gluon fields  $\psi$  and  $A$  at every point in space-time. Discretisation of space-time onto a lattice makes the number of space-time points (and therefore field variables) finite. Continuous space-time  $(x, t)$  becomes a grid of labelled points,  $(x_i, t_i)$  or  $(n_i a, n_t a)$  where  $a$  is the lattice spacing (this doesn't have to be the same in all directions but usually is). The fields are then associated only with the sites,  $\psi(x, t) \rightarrow \psi(n_i, n_t)$ . The action must also be discretised, but, as in the previous section, this is straightforward, replacing fields by fields at the lattice sites and the derivatives by finite differences of these fields. The integral over space-time of the Lagrangian becomes a sum over all lattice sites:  $(\int d^4x \rightarrow \sum_n a^4)$ , and the path integral becomes a product of integrals over each of the fields, to be done by Monte Carlo averaging. These integrals will be finite, unlike such integrals in the continuum, because the lattice provides a regularisation of the theory. The lattice spacing provides an ultra-violet cut-off in momentum space since no momenta larger than  $\pi/a$  make sense (since the wavelength is then smaller than  $a$ ).

To discretise gauge theories such as QCD onto a lattice in fact requires a little additional thought to that described above because of the paramount importance of local gauge invariance. The rôle of the gluon (gauge) field in QCD is to transport colour from one place to another so that we can rotate our colour basis locally. It should then seem natural for the gluon fields to 'live' on the links connecting lattice points, if the quark fields 'live' on the sites.

The gluon field is also expressed somewhat differently on the lattice to the continuum. The continuum  $A_\mu$  is an 8-dimensional vector, understood as a product of coefficients  $A_\mu^b$  times the 8 matrices,  $T_b$ , which are generators of the SU(3) gauge group for QCD. On the lattice it is more useful to take the gluon field on each link to be a member of the gauge group itself *ie* a special (determinant = 1) unitary  $3 \times 3$  matrix. The lattice gluon field is denoted  $U_\mu(n_i, n_t)$ , where  $\mu$  denotes the direction of the link,  $n_i, n_t$  refer to the lattice point at the beginning of the link, and the colour indices are suppressed. We will often just revert to continuum notation for space-time, as in  $U_\mu(x)$ . The lattice and continuum fields are then related exponentially,

$$U_\mu = e^{-iagA_\mu} \quad (12)$$

where the  $a$  in the exponent makes it dimensionless, and we include the coupling,  $g$ , for convenience. If  $U_\mu(x)$  is the gluon field connecting the points  $x$  and  $x+1_\mu$  (see Figure 3), then the gluon field connecting these same points but in the downwards direction must be the inverse of this matrix,  $U_\mu^{-1}(x)$ . Since the  $U$  fields are unitary matrices, satisfying  $U^\dagger U = 1$ , this is then  $U_\mu^\dagger(x)$ .

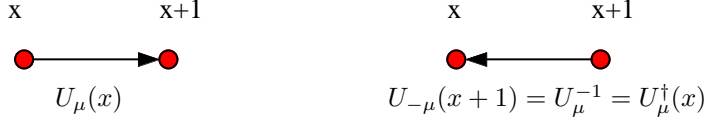


**Figure 3.** The gluon field on the lattice.

This form for the gluon field makes it possible to maintain exact local gauge invariance on a lattice. To apply a gauge transformation to a set of gluon fields we must specify an  $SU(3)$  gauge transformation matrix at each point. Call this  $G(x)$ . Then the gluon field  $U_\mu(x)$  simply gauge transforms by the (matrix) multiplication of the appropriate  $G$  at both ends of its link. The quark field (a 3-dimensional colour vector) transforms by multiplication by  $G$  at its site.

$$\begin{aligned} U_\mu^{(g)}(x) &= G(x)U_\mu(x)G^\dagger(x+1_\mu) \\ \psi^{(g)}(x) &= G(x)\psi(x) \\ \bar{\psi}^{(g)}(x) &= \bar{\psi}(x)G^\dagger(x). \end{aligned} \quad (13)$$

To understand how this relates to continuum gauge transformations try the exercise of setting  $G(x)$  to a simple  $U(1)$  transformation,  $e^{-i\alpha(x)}$ , and show that Equation 13 is equivalent to the QED-like gauge transformation in the continuum,  $A_\mu^g = A_\mu - \partial_\mu\alpha$ .

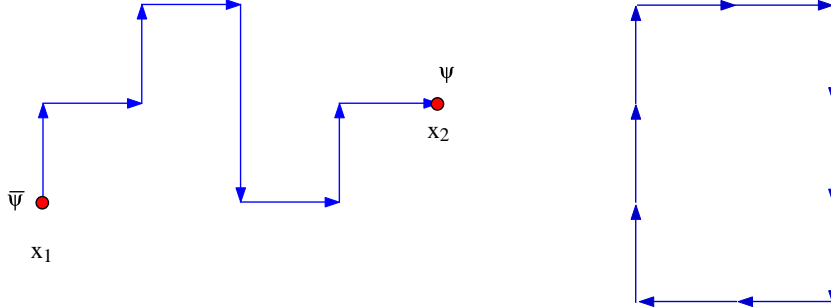


**Figure 4.** A string of gluon fields connecting quark and antiquark fields (left) and a closed loop of gluon fields (right).

Gauge-invariant objects can easily be made on the lattice (see Figure 4) out of closed loops of gluon fields or strings of gluon fields with a quark field at one end and an antiquark field at the other, eg  $\bar{\psi}(x_1)U_\mu(x_1)U_\nu(x_1+1_\mu)\dots U_\epsilon(x_2-1_\epsilon)\psi(x_2)$ . Under a gauge transformation the  $G$  matrix at the beginning of one link ‘eats’ the  $G^\dagger$  at the end of the previous link, since  $G^\dagger G = 1$ . The  $G$  matrices at  $x_1$  and  $x_2$  are ‘eaten’ by those transforming the quark and anti-quark fields, if we sum over quark and antiquark colours.

The same thing happens for any closed loop of  $U$ s, provided that we take a trace over colour indices. Then the  $G$  at the beginning of the loop and the  $G^\dagger$  at the end of the loop, the same point for a closed loop, can ‘eat’ each other.

The purely gluonic piece of the continuum QCD action is

$$S_{\text{cont}} = \int d^4x \frac{1}{2} \text{Tr} F_{\mu\nu} F^{\mu\nu} \quad (14)$$

where  $F_{\mu\nu}$  is the field strength tensor,

$$F_{\mu\nu} = \partial_\mu A_\nu - \partial_\nu A_\mu + ig[A_\mu, A_\nu]. \quad (15)$$

The simplest lattice discretisation of this is the so-called Wilson plaquette action:

$$S_{\text{latt}} = \beta \sum_p \left( 1 - \frac{1}{3} \text{Re} \{ \text{Tr} U_p \} \right); \quad \beta = \frac{6}{g^2}. \quad (16)$$

In fact the 1 here is irrelevant in the lattice QCD calculation, giving only an overall normalisation that vanishes from the ratio of path integrals, and so it is often dropped from  $S_{\text{latt}}$ .

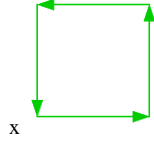


**Figure 5.** A plaquette on the lattice.

$U_p$  is the closed  $1 \times 1$  loop called the plaquette, an  $SU(3)$  matrix formed by multiplying 4 gluon links together in a sequence. For the plaquette with corner  $x$  in the  $i, j$  plane we have (Figure 5):

$$U_{p,ij}(x) = U_i(x)U_j(x+1_i)U_i^\dagger(x+1_j)U_j^\dagger(x) \quad (17)$$

$\text{Tr}$  in  $S_{\text{latt}}$  denotes taking the trace of  $U_p$  ie the sum of the 3 diagonal elements.  $S_{\text{latt}}$  sums over all plaquettes of all orientations on the lattice.  $\beta$  is a more convenient version for the lattice of the QCD bare coupling constant,  $g^2$ . This is the single input parameter for a QCD calculation (whether on the lattice or not) involving only gluon fields. Notice that the lattice spacing is not explicit anywhere, and we do not know its value until *after* the calculation. (This is a difference from the quantum mechanical example of the previous section where we had to choose and input a value for  $a$ .) The value of the lattice spacing depends on the bare coupling constant. Typical values of  $\beta$  for current lattice calculations using the Wilson plaquette action are  $\beta \approx 6$ . This corresponds to  $a \approx 0.1\text{fm}$ . Smaller values of  $\beta$  give coarser lattices, larger ones, finer lattices. This is obvious from the asymptotic freedom of QCD, which tells us that the coupling constant  $g^2$  goes to zero at small distances or, equivalently, high energies.  $\beta$  is the inverse of the bare coupling constant at the scale of the lattice spacing and therefore tends to  $\infty$  as the lattice spacing goes to zero.



That  $S_{\text{latt}}$  of Equation 16 is a discretisation of  $S_{\text{cont}}$  is not obvious, and we will not demonstrate it here. It should be clear, however, from Equations 12 and 17 that  $S_{\text{latt}}$  does contain terms of the form  $\partial_\mu A_\nu$  needed for the field strength tensor,  $F_{\mu\nu}$ .

$S_{\text{latt}}$  is gauge-invariant, as will be clear from earlier. Thus lattice QCD calculations do *not* require gauge fixing or any discussion of different gauges or ghost terms, as would be required for continuum calculations using perturbation theory. Our lattice calculation is fully non-perturbative since the Feynman Path Integral includes any number of QCD interactions. In contrast to the real world, however, the calculations are done with a non-zero value of the lattice spacing and a non-infinite volume. In principle we must take  $a \rightarrow 0$  and  $V \rightarrow \infty$  by extrapolation. In practice it suffices to demonstrate, with calculations at several values of  $a$  and  $V$ , that the  $a$  and  $V$  dependence of our results is small, and understood, and include a systematic error for this in our result.

Before discussing quarks we illustrate here how a lattice calculation is done with only gluon fields, how the lattice spacing is determined, and what the systematic errors are.

A quantity that can be calculated in the pure gluon theory is the expectation value of a closed loop of gluon fields. In fact this can be related to the QCD potential between an infinitely massive quark and antiquark. Although not directly a physical quantity, this is something about which we have some physical understanding. An infinitely massive quark does not move in spatial directions and so simply generates a path which is a string of gluon fields in the time direction. If this is joined to a string generated by an antiquark a distance  $R$  in lattice units away then a rectangular  $R \times T$  loop of gluon fields is created. This is known as a Wilson loop, see Figure 4 right.

To ‘measure’ this in pure gluon QCD, we generate configurations of gluon fields with probability  $e^{-S_{\text{latt}}}$  where  $S_{\text{latt}}$  is a discretisation of the pure gluon QCD action given by Equation 16. On each of these configurations we calculate the  $R \times T$  Wilson loop, averaging over all positions of it on the lattice. We then average over the results on each configuration in the ensemble to obtain a final answer with statistical error, for lots of values of  $R$  and  $T$ . We have

$$\frac{1}{Z} \langle 0 | \mathcal{O} | 0 \rangle = \frac{\int \mathcal{D}U \mathcal{O}[U] e^{-S_{g,QCD}}}{\int \mathcal{D}U e^{-S_{g,QCD}}} = \langle \langle \mathcal{O} \rangle \rangle = \frac{1}{N_{\text{conf}}} \sum_{i=1}^{N_{\text{conf}}} O_i \quad (18)$$

Typically we need many hundreds of configurations in an ensemble for a small statistical error at large  $R$  and  $T$ .

The ensemble average of  $O$  is related to the heavy quark potential by similar arguments to those used for the operator  $x(t_1)x(t_1)$  in section 2.1. One end of the Wilson loop creates a set of eigenstates of the Hamiltonian that are based on a massive quark-antiquark pair. These eigenstates are produced with different amplitudes by the Wilson loop operator and have different energies. In this case there is no kinetic energy, so the energies are those of the heavy quark potential. The different eigenstates propagate for time  $T$  and, if  $T$  is large, the ground state eventually dominates.

$$\langle \langle \mathcal{O} \rangle \rangle = C e^{-aV(R)T} + C' e^{-aV'(R)T} + \dots \quad (19)$$

By fitting the results as a function of the time length,  $T$ , in lattice units, the heavy quark potential in lattice units,  $aV(R)$ , is obtained.  $V'$  is some kind of excitation of the potential which we will not be interested in here. The heavy quark potential at short distances

should behave perturbatively and take a Coulomb form. At large distances we expect a ‘string’ to develop which confines the quark and antiquark and gives a potential which rises linearly with separation. We can therefore fit the lattice potential to the form

$$aV(r = Ra) = -\frac{4}{3} \frac{\alpha_s(r)}{R} + \sigma a^2 R + \tilde{C} \quad (20)$$

where  $\tilde{C}$  is a ‘self-energy’ constant that appears in the lattice calculation. If the results for  $aV(R)$  are plotted against  $R$ , the slope at large  $R$  is the ‘string tension’,  $\sigma$ , in lattice units, *ie*  $\sigma a^2$ . Phenomenological models of the heavy quark potential give values for  $\sqrt{\sigma}$  of around 440 MeV. Using this value for  $\sigma$  and the result from the lattice of  $\sigma a^2$ , gives a value for  $a$ . This is often quoted as a value for  $a^{-1}$  in GeV. Note that  $a^{-1}$  in GeV = 0.197/( $a$  in fm).

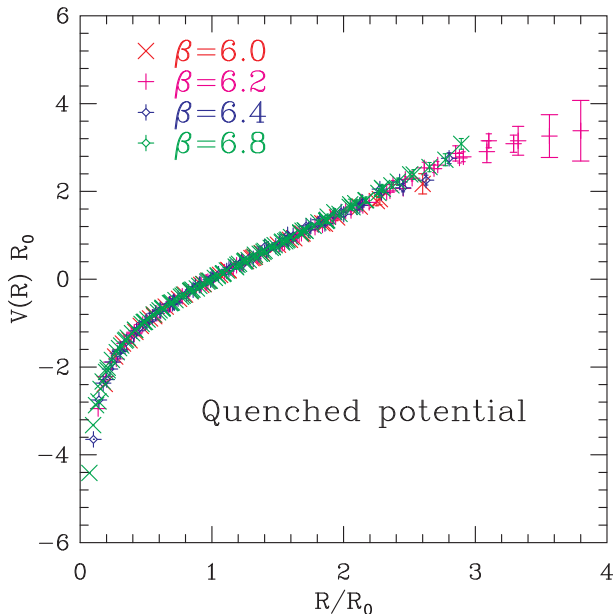


**Figure 6.** The heavy quark potential in units of the parameter,  $r_0$ , as a function of distance,  $r$ , also in units of  $r_0$ . The calculations were done in quenched (pure glue) QCD at a variety of different values of the lattice spacing, corresponding to the different values of  $\beta$  quoted. (Bali 2000)

The results for  $aV$  can then be multiplied by  $a^{-1}$  to convert them to physical units of GeV and, having removed the constant  $\tilde{C}$ , the results can be plotted as a function of the physical distance,  $r$  in fm. If discretisation errors are small, then results at different values of the lattice spacing should be the same. Figure 6 shows results for the heavy quark potential on relatively fine lattices at different values of  $\beta$  using the Wilson plaquette action for  $S_g$  (Bali 2000).  $V(r)$  is not in fact given in GeV here, nor is  $r$  in fm, but both are given in terms of a parameter called  $r_0$  (Sommer 1994). This is the value of  $r$  at which  $r^2 \partial V / \partial r = 1.65$  and is a commonly used quantity to determine the lattice spacing (or at least relative lattice spacings), rather than the string tension.  $r_0$  is not a physical

parameter, and as such is not available in the Particle Data Tables. We shall see later that there are good hadron masses to use for the determination of  $a$  and these can also be used to determine the value of  $r_0$ . Meanwhile,  $r_0 \approx 0.5\text{fm}$ . The results at different values of  $\beta$  lie on top of each other and this gives us confidence that the discretisation errors are small.

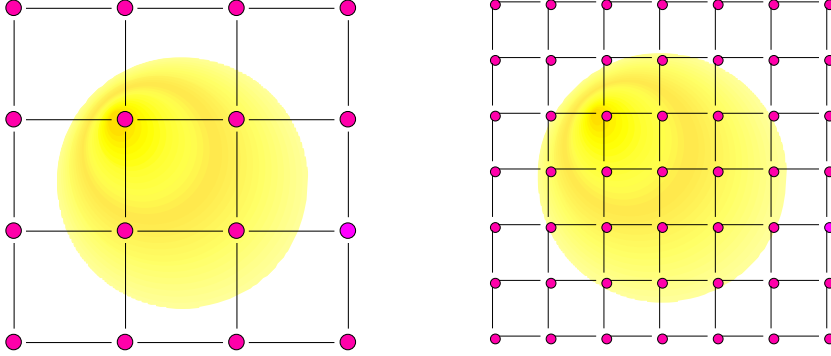


**Figure 7.** A physical object on two lattices of different lattice spacing. On the right our updating algorithm takes much longer to register a significant change on the length scale of the object.

The values of  $\beta$  used correspond to rather fine lattices. The coarsest lattice is at  $\beta = 6.0$  and has  $a=0.1\text{fm}$ . The finest lattice is at  $\beta = 6.8$  and has  $a = 0.03\text{fm}$ . The finest configurations are very expensive to generate. Yet if we looked closely at the results at  $\beta = 6.0$  we would be able to see discretisation errors at the few percent level. If we want accurate results on lattices that are coarse enough for affordable calculation (especially, as we shall see, once we include quarks) then we must improve the discretisation of the action. The cost of lattice calculations grows naively as  $a^{-4}$  because of the four-dimensional space-time. In fact it is even worse than this because of critical slowing-down. Physical distances on the lattice grow in lattice units as the lattice spacing gets smaller (see Figure 7). This means that algorithms that update configurations by making local changes to the fields, get slower and slower at making a change on a distance scale of  $r$  as  $a$  is reduced. Then the cost of the calculation of, say,  $V(r)$  actually grows as  $a^{-6}$ . It becomes imperative to improve the action, rather than to attempt to beat down the discretisation errors by reducing  $a$ .

Improving the gluon action is at first sight straightforward. We expand the Wilson plaquette action in powers of  $a$  and notice that it has  $a^2$  errors when compared to the continuum QCD gluon action. We add a higher dimension operator to the action in the form of a  $2 \times 1$  Wilson loop to cancel this error:

$$S_{g,latt} = \beta \sum \left( 1 - \frac{5c_1}{3} \frac{\text{ReTr}U_p}{3} + \frac{c_2}{12} \frac{\text{ReTr}(U_{2 \times 1} + U_{1 \times 2})}{3} \right). \quad (21)$$

$c_1$  and  $c_2$  are chosen to remove the  $a^2$  error and naively would have the value 1. However, in a quantum field theory like QCD, the value of  $c_{1,2}$  becomes renormalised by radiative corrections.  $S_{g,latt}$  must reproduce  $S_{g,cont}$  to a required level of accuracy and so  $c_{1,2}$  must absorb the effect of the differences in gluon radiation between the continuum

and lattice versions of QCD. This difference arises from gluon radiation with momentum larger than  $\pi/a$  which does not exist on the lattice. Gluon radiation at these high momenta is perturbative and so we can calculate  $c_{1,2}$  as a perturbative power series in  $\alpha_s$ . Provided  $a$  is small enough so that  $\alpha_s(\pi/a)$  is small enough, the  $c_{1,2}$  will not be very different from 1. There is a complication, however, and that arises from the way in which the lattice gluon field  $U_\mu$  is related to the usual gluon field  $A_\mu$ . The exponential relationship in Equation 12 means that the lattice perturbation theory contains vertices with many powers of  $A_\mu$ . Although these are suppressed by powers of  $g$ , they produce rather large contributions and have to be taken into account. In fact they appear as so-called ‘tadpole’ diagrams which take the same form in many different processes (Lepage and Mackenzie 1993). This allows them to be substantially removed in a universal way by the simple expedient of estimating how far the gluon link field,  $U_\mu$ , is from the value 1 (the  $3 \times 3$  unit matrix) that it would take in the continuum,  $g^2 \rightarrow 0$  limit. We can measure this, for example, from the average plaquette (traced and divided by 3 so that it would be 1 in the continuum limit). This contains 4  $U$  fields so we take the fourth root to determine the ‘tadpole-factor’,  $u_0$ . Taking

$$U_\mu(x) \rightarrow \frac{U_\mu(x)}{u_0} \quad (22)$$

is called ‘tadpole-improvement’. If this is done then the calculation of  $c_{1,2}$  does indeed give well-behaved perturbative expansions which do not differ substantially from the naive value of 1. The improved gluon action becomes

$$S_{g,latt} = \beta \sum \left( -\frac{5c_1}{3} \frac{\text{ReTr}U_p}{3u_0^4} + \frac{c_2}{12} \frac{\text{ReTr}(U_{2 \times 1} + U_{1 \times 2})}{3u_0^6} \right), \quad (23)$$

dropping the constant term in the action. Taking  $c_{1,2}$  to be 1 is the tree-level tadpole-improved Symanzik action and this gives results significantly better than the Wilson plaquette action on coarse lattices (Alford *et al.* 1995, Lepage 1996). Note that  $\beta$  here cannot be compared directly to that for the Wilson plaquette action. It only makes sense to compare results between different actions at the same value of the lattice spacing.

Figure 8 compares results for the heavy quark potential, calculated as discussed above, for the two actions on coarse lattices with lattice spacing 0.4fm (Alford *et al.* 1995). The results with the Wilson plaquette action show clear discretisation errors in the fact that  $V(r)$  is not a smooth curve, *ie* it does not have rotational invariance. It reflects the fact that distances on the lattice are not in general travelled in straight lines and the result will depend on the actual path used between two points. The curve obtained with the improved gluon action is much smoother. As discretisation errors are removed, the path dependence of the distance measurement is reduced and the rotational invariance of the continuum is restored. Indeed  $c_{1,2}$  could be fixed non-perturbatively (*ie* within the lattice simulation) by demanding rotational invariance and it is clear from this that results close to 1 after tadpole-improvement would be obtained.

In section 3 we will describe recent lattice results and these use an improved gluon action to reduce the discretisation errors. In fact the action is improved beyond that used in Figure 8 by including the first  $\alpha_s$  terms in  $c_1$  and  $c_2$  and an additional operator that appears at  $\mathcal{O}(\alpha_s)$  made of a 3-dimensional parallelogram of  $U$  fields (Alford *et al.* 1995, Lepage 1996).

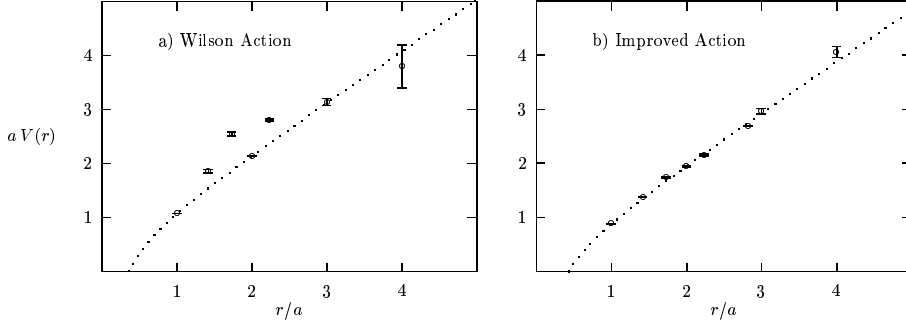


**Figure 8.** The heavy quark potential calculated in pure gluon QCD at a lattice spacing,  $a$ , of  $0.4\text{fm}$ . The left plot uses the Wilson plaquette action, the right plot the tree-level tadpole-improved Symanzik action. The right plot has a much smoother curve than the upper one reflecting the improvement of discretisation errors (Alford et al. 1995).

### 2.3 Quark fields in Lattice QCD

Quarks represent a big headache for Lattice QCD. Because quark fields anticommute, they cannot be handled using ordinary numbers on a computer. We therefore have to perform the integral over the quark fields in the path integral by hand. In fact this is easy to do because of the way that the quark fields appear in the QCD action. Including the Dirac piece of the action for quarks, we have

$$\begin{aligned} Z &= \int \mathcal{D}U \mathcal{D}\psi \mathcal{D}\bar{\psi} e^{-S_{QCD}} \\ S_{QCD} &= S_g + \sum_x \bar{\psi}(\gamma \cdot D + m)\psi = S_g + \bar{\psi}M\psi. \end{aligned} \quad (24)$$

The quark field,  $\psi$  is a 12-component (3 for colour and 4 for spin) field at every lattice point, so  $M$  is a matrix with  $12 \times L^3T$  rows and columns for an  $L^3T$  lattice.  $D$  is a covariant derivative that includes a coupling with the gluon field. The integral over quark fields gives

$$Z = \int \mathcal{D}U \det(M) e^{-S_{g,QCD}} = \int \mathcal{D}U e^{-\tilde{S}_{QCD}} \quad (25)$$

where  $\tilde{S} = S_{g,QCD} + \ln \det(M)$ , one  $\det M$  factor per quark flavour.

Typically in lattice QCD we want to calculate the mass of a hadron made of quarks and antiquarks. To do this we must calculate the expectation value of a product of appropriate operators made of quarks and antiquarks. A suitable operator that creates a meson is  $\bar{\psi}^{a,\alpha,f_1} \Gamma^{\alpha\beta} \psi^{a,\beta,f_2}$  where  $\Gamma$  is some combination of  $4 \times 4$   $\gamma$  matrices that give the right spin-parity ( $J^P$ ) quantum numbers to the meson,  $a$  is a colour index,  $\alpha$  and  $\beta$  are spin indices and  $f_i$  are flavour indices. We include the conjugate operator to destroy the meson  $T$  lattice spacings away in time. Then, suppressing colour and spin,

$$\frac{1}{Z} \langle 0 | H^\dagger(T) H(0) | 0 \rangle = \frac{\int \mathcal{D}U \mathcal{D}\psi \mathcal{D}\bar{\psi} (\sum_{\vec{x}} \bar{\psi}^{f_1} \Gamma \psi^{f_2}(\vec{x}))_T (\bar{\psi}^{f_2} \Gamma \psi^{f_1})_0 e^{-S_{QCD}}}{\int \mathcal{D}U \mathcal{D}\psi \mathcal{D}\bar{\psi} e^{-S_{QCD}}}. \quad (26)$$

On integration, the right-hand-side becomes (for the case where  $f_1 \neq f_2$ ):

$$\frac{\int \mathcal{D}U \text{Tr}_{\text{spin,colour},\bar{x}}(M_{f_1(0,T)}^{-1} \Gamma M_{f_2(T,0)}^{-1} \Gamma) \det M e^{-S_g, QCD}}{\int \mathcal{D}U \det M e^{-S_g, QCD}}. \quad (27)$$

This calculation requires us to generate sets of gluon field configurations with probability  $e^{-\tilde{S}_{QCD}}$ , calculate the trace over spin and colour of the  $M^{-1}$  factors on each configuration and then average these over the ensemble. The calculation is illustrated in Figure 9. It is known as a 2-point function calculations because there are two operators at times 0 and  $T$ , represented by the filled ovals. The straight lines at the top and bottom indicate the valence quark propagators (the  $M^{-1}$  factors above that connect the creation and annihilation operators for that particular valence quark). As the quark propagates it interacts any number of times with the other quark through the lattice gluon field and this is indicated by the curly lines. Some of these gluon lines may include the effect of a sea quark-antiquark pair (as on the left of the diagram).

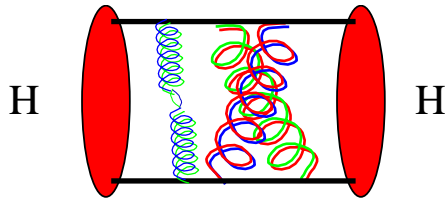


**Figure 9.** An illustration of the calculation of a simple 2-point function for a hadron in lattice QCD.

If we have  $f_1 = f_2$  for a flavour-singlet quantity then there are additional ‘disconnected’ pieces where the  $M^{-1}$  factors are generated from each operator separately. This gives, for example,  $\text{Tr}(M_{(0,0)}^{-1})\text{Tr}(M_{(T,T)}^{-1})$ . These are very difficult to calculate, being very noisy, and accurate results for light flavour-singlet mesons are not yet available. For heavy mesons,  $c\bar{c}$  and  $b\bar{b}$ , this is expected to be a very small effect and is usually ignored.

The hadron mass is determined from the results through the usual multi-exponential form

$$\frac{1}{Z} \langle |0H^\dagger(T)H(0)|0 \rangle = \langle \langle \text{Tr}_{\text{spin,colour},\bar{x}}(M_{f_1}^{-1} \Gamma M_{f_2}^{-1} \Gamma) \rangle \rangle = \sum_n C_n e^{-m_n a T}. \quad (28)$$

$n$  runs over radial excitations of the hadron with a particular set of  $J^P$  and flavour quantum numbers, and  $m_n a$  are the different hadron masses. In fact the formula above is only correct for a lattice of infinite time extent in lattice units,  $T'$ . On the finite lattices we must use there are additional terms from the possibility of quarks ‘going backwards’ round the lattices. These terms take the form  $e^{-m_n a(T'-T)}$  and can readily be taken account of in the fit, although their form does depend on the hadron being studied.  $C_n$  in the above equation is related to the square of the matrix element  $\langle 0|H|n \rangle$  by analogy with Equation 8 in section 2.1. The size of  $C_n$  then depends on the form of the operator  $H$  used to create and destroy the hadron. Any operator with the right quantum numbers can be used and if we make a set of such operators we can calculate a whole matrix of

correlators and fit them simultaneously for improved precision. Typically we use operators made of quark and antiquark fields but separated in space according to some kind of ‘wavefunction’, (known as a ‘smearing’) *eg*  $\bar{\psi}_x \phi(x-y) \psi_y$ . To make a gauge-invariant operator of this kind either requires strings of  $U$ s to be inserted between  $x$  and  $y$  or for the gluon field configuration to be gauge-fixed, typically to Coulomb gauge. It may be possible to choose  $\phi$  so that a particularly good overlap with one of the states of the system (*eg* the ground state) is obtained, and poor overlap with the others. Then  $C_0$  would be large in the equation above, and the other  $C_n$  small, and this would give improved precision for  $m_0 a$ . The masses of the radial excitations are of interest too and smearings which improve overlap with them have also been studied. With particular operators,  $H$ ,  $C_n$  contains information of physical relevance. For example the matrix element of the temporal axial current,  $J_{A_0}$  between the vacuum and a pseudoscalar meson gives its decay constant, related to the rate for its decay purely to leptons via a  $W$  boson. The calculation in lattice QCD of matrix elements of this kind is discussed in section 3.3.

The way in which a lattice QCD calculation with quarks is done makes a clear distinction between valence quarks and sea quarks. The valence quarks are those that give the hadron its quantum numbers and these give rise to the  $M^{-1}$  factors in Equation 27. The sea quarks are those that are produced as quark-antiquark pairs from energy fluctuations in the vacuum (quark vacuum polarisation). They give rise to the  $\det M$  factors in Equation 27. The important sea quarks are the light ones,  $u$ ,  $d$  and  $s$ . The heavy quarks  $c$  and  $b$  have no effect as sea quarks and the  $t$  quark does not even have to be considered as a valence quark since it does not form bound states before decaying.

Manipulations of the matrix  $M$  are computationally costly. Even though it is a sparse matrix (with only a few non-zero entries) it is very large. There are various computational techniques for calculating the  $M^{-1}$  factors and the  $\det M$  factor is included by repeated determination of the calculation of  $M^{-1}$ . This makes the inclusion of  $\det M$  very costly indeed. It becomes increasingly hard as the quark mass becomes smaller because  $M$  becomes ill-conditioned. (The eigenvalues of  $M$  range between some fixed upper limit and the quark mass, so this range increases as  $m_q \rightarrow 0$ ). In the real world the  $u$  and  $d$  quarks have very small mass and so in the past there has not been sufficient computer power available to include them as sea quarks or, if they have been included, their masses have been much heavier than their real values.

Missing out sea quarks entirely is known as the quenched approximation. It is clearly wrong, but for a long time the presence of other systematic errors and poor statistics obscured this fact. More recently it has become clear that the systematic error in the quenched approximation is around 10-20%. When light quark vacuum polarisation ( $\det M$ ) is included the calculation is said to be ‘unquenched’ or ‘dynamical’. The sea quarks are then also called dynamical quarks. We will see in the results section that it is now possible to include realistic quark vacuum polarisation effects and the quenched approximation can be laid aside at last.

Our earlier discussion makes clear that the computational cost of including light quark vacuum polarisation will require a very good (*ie* highly improved) discretisation of both the gluon and quark actions. We have discussed the gluon action earlier. For the quark action there are several possibilities, or formulations. We will concentrate here on those formulations that have already been used in unquenched simulations.

The naive quark action is a straightforward discretisation of the Dirac action in Eu-

clidean space-time:

$$S_q = \sum_x \bar{\psi}(x)(\gamma \cdot \Delta + ma)\psi(x). \quad (29)$$

The finite difference  $\Delta$  is

$$\Delta_\mu \psi(x) \equiv \frac{1}{2}(U_\mu(x)\psi(x + 1_\mu) - U_\mu^\dagger(x - 1_\mu)\psi(x - 1_\mu)) \quad (30)$$

showing explicitly how the gluon fields appear, coupled to the quarks, to maintain gauge invariance in the action. QCD with quarks has parameters, in addition to the coupling constant, that are the quark masses. In lattice QCD these appear as quark masses in lattice units,  $ma$ . As with the lattice spacing/coupling constant, the quark masses are not known a priori and must be adjusted as a result of a lattice calculation. We therefore iterate until, for example, we get a particular hadron mass correct. Since the quark mass is in lattice units, finer lattices will require smaller values of  $ma$  than coarser ones.

The naive quark action has several good properties. It has discretisation errors at  $\mathcal{O}(a^2)$ . The finite difference piece is anti-hermitian and therefore has purely imaginary eigenvalues that appear as  $\pm i\lambda$ . With the mass term the eigenvalues of  $M$  are then  $ma \pm i\lambda$ . This is the same as in the continuum and follows from the chiral symmetry of the action *ie* our ability to rotate independently left- and right- handed projections of the quark field. It means that the bare quark mass is simply multiplicatively renormalised and the renormalised quark mass goes to zero at the same point as the bare quark mass. This is important because we need to work with very small (renormalised) quark masses for the  $u$  and  $d$  quarks and we want to be able to go in that direction by just taking  $ma$  to be smaller and smaller (if we have enough computing power).

Chiral symmetry is spontaneously broken in the real world giving rise to a Goldstone boson, the  $\pi$ , whose mass consequently vanishes at zero quark mass ( $m_\pi^2 \propto m_q$ ). For small quark masses, where  $m_\pi$  is small, we have a well-developed chiral perturbation theory which tells us how hadron masses and properties should depend on the  $u/d$  quark masses (or equivalently  $m_\pi^2$ ) and we can make use of this to extrapolate down to physical  $u/d$  quark masses from the results of our lattice QCD simulation provided that we are able to work at small enough  $u/d$  quark masses to be in the regime where chiral perturbation theory works. In general  $m_{u/d} < m_s/2$  is necessary for an accurate extrapolation. We will discuss this further in section 3. (Arndt 2004)

It would seem that we have everything ready to do the simulations but we must first discuss the infamous doubling problem. The naive quark action in fact describes 16 quarks rather than 1. This is demonstrated most easily in 1-dimension in the absence of gluon fields. It suffices to compare the continuum derivative in momentum space, *ie*  $p$ , with the Fourier transform of the finite difference on the lattice, which is  $\sin(pa)/a$ . These are plotted in Figure 10 as a function of  $p$  between  $-\pi/a$  and  $\pi/a$ , the limits over which  $p$  makes sense on the lattice (the first Brillouin zone). Momenta larger than  $\pi/a$  reappear as negative momenta larger than  $-\pi/a$  so these points are periodically connected. Around  $p \approx 0$  the sine function goes through zero and mimics a straight line up to  $a^2$  errors as expected. The problem is that this is also true around  $p \approx \pi/a$  (with opposite slope). This means that there is a continuum-like solution of the Dirac equation around  $p = \pi/a$  as well as around  $p = 0$  *ie* there are 2 quarks instead of 1. In 4-d (and including  $\gamma$  matrix algebra as well) the picture is more complicated but the basic



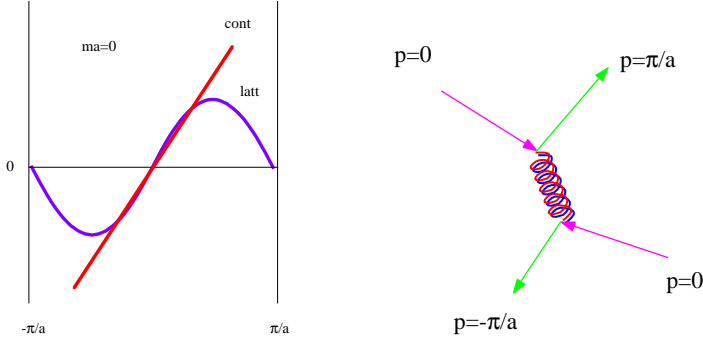


**Figure 10.** (Left) The continuum derivative and lattice finite difference compared as a function of momentum within the first Brillouin zone on the lattice. The points  $p = \pi/a$  and  $-\pi/a$  are joined by lattice periodicity. (Right) Taste-changing interactions for naive quarks. A high-momentum ( $p = \pi/a$ ) gluon exchange can change one taste of quark into another.

facts are the same - there are  $2^4$  quarks instead of 1. The ‘doublers’ or extra ‘tastes’ of quark live at the edges of the Brillouin zone, where any component of  $p$  is close to  $\pi/a$ .

This was originally thought to be disastrous and huge efforts, which continue today, were made to solve the problem. Wilson introduced a Wilson term into the naive action which has the effect of giving mass to the doublers. The Wilson action is then

$$S_f^W = S_f^{naive} - \frac{r}{2} \sum_x \bar{\psi}_x \square \psi_x$$

$$\square \psi_x = \sum_{\mu=1}^4 U_\mu(x) \psi_{x+1_\mu} - 2\psi_x + U_\mu^\dagger(x-1_\mu) \psi_{x-1_\mu}. \quad (31)$$

In the absence of gluon fields the Fourier transform of the extra term is  $2r \sin^2(pa/2)$  which has a maximum at  $\pm\pi/a$ . When folded in to the inverse quark propagator, taking account of the  $\gamma$  matrix structure, this then prevents the inverse propagator from vanishing at the edges of the Brillouin zone, effectively giving the doublers a large mass which increases as  $a \rightarrow 0$  so that they are completely removed in the continuum limit.

This solution of the doubling problem was used for many years. It does have two big disadvantages. One is that discretisation errors now appear at  $\mathcal{O}(a)$  which causes large systematic errors even on relatively fine lattices. The other is that the Wilson term does not respect chiral symmetry and so we lose the simple connection between the bare quark mass parameter and the renormalised quark mass and have to search in  $ma$  for the point where  $m_\pi$  vanishes. The eigenvalue spectrum is now complicated as well which creates numerical difficulties. Discretisation errors are ameliorated in the improved form of the action known as the ‘clover’ action. The  $\mathcal{O}(a)$  errors are cancelled by a  $\sigma_{\mu\nu} F^{\mu\nu}$  term which is discretised as a set of plaquettes around a central point that looks like a 4-leaf clover. The coefficient of the clover term can be set using tadpole-improvement or non-perturbatively. Again it is close to 1 *after* the tadpole-improvement with a well-behaved perturbative expansion. Work using the clover action continues and it is being used

for unquenched simulations (Ishikawa *et al.* 2005). A newer form of the action, called twisted mass QCD, is also being developed. This overcomes several of the numerical problems and is a promising development for the future (Frezzotti 2005).

Another relatively new development is that of a set of actions that maintain chiral symmetry on the lattice but also solve the doubling problem. These require an enormous increase in computer power because they either need a matrix inversion inside a matrix inversion to calculate  $M^{-1}$  (overlap quarks) or a calculation in 5-dimensions (domain wall quarks). Calculations using these formalisms have then been restricted to the quenched approximation because of the cost. In future they may be possible to implement including realistic quark vacuum polarisation effects on very powerful supercomputers (Chiu 2004).

The recent progress in lattice QCD calculations has come, however, from returning to the naive discretisation of the quark action. In fact the doubling problem is not a problem if the doublers are simply copies of each other, because we can then simply ‘divide by 16’ inside our calculation. If  $M$  has a 16-fold degeneracy in its eigenvalue spectrum then taking  $(\det M)^{1/16}$  gives us the effect of 1 taste for each flavour. The problem is that the different tastes of quarks do interact with each other and change taste and this splits some of the degeneracy. The process by which this happens is a high momentum ( $\pi/a$ ) gluon exchange as in Figure 10 which moves the quark from one Brillouin zone boundary to another. These taste-changing interactions are an artefact of using the lattice and they induce large discretisation errors, even though they are formally  $\mathcal{O}(a^2)$  (Lepage 1998b). To improve the naive action then requires removing the unphysical taste-changing interactions at leading order as well as the usual  $a^2$  errors from discretising a derivative as a symmetric finite difference, discussed in section 2.1. This markedly improves the discretisation errors, but also significantly reduces the taste-changing interactions, and makes this action a good one for lattice simulations.

The naive quark formalism is fast numerically because it can be converted to the staggered quark formalism in which there is no quark spin. It is a remarkable feature that the quark fields can be rotated so that the naive quark action (or its improved variant) is diagonal in spin space. We have only to simulate one spin component on the lattice and then, if required, we can reconstruct all quantities in terms of naive quarks. If we take

$$\psi(x) \rightarrow \Omega(x)\chi(x); \quad \bar{\psi}(x) \rightarrow \bar{\chi}(x)\Omega^\dagger(x) \quad (32)$$

where

$$\Omega(x) \equiv \prod_{\mu=0}^3 (\gamma_\mu)^{x_\mu},$$

the unimproved naive action becomes

$$\bar{\psi}(x)(\gamma \cdot \Delta + ma)\psi = \bar{\chi}(x)(\alpha(x) \cdot \Delta + ma)\chi(x)$$

where  $\alpha(x)$  is diagonal in spin space,  $\alpha_\mu(x) = (-1)^{x_0 + \dots + x_{\mu-1}}$ . Rewriting the action in terms of a single-spin (but 3-colour) component field  $\chi$ , we have the unimproved staggered quark action:

$$S_f^S = \sum_x \bar{\chi}_x \left\{ \frac{1}{2} \sum_\mu \alpha_{x,\mu} (U_\mu(x)\chi_{x+1_\mu} - U_\mu^\dagger(x-1_\mu)\chi_{x-1_\mu}) + ma\chi_x \right\}. \quad (33)$$

The staggered quark action does not solve the doubling problem, but removes an exact 4-fold degeneracy from it. There are then 4 tastes for every quark flavour that we include with  $M$  instead of 16. If we improve the action so that the  $a^2$  taste-changing interactions are small then the tastes will be close to being copies of each other. We will expect to see a 4-fold close-to-degeneracy in the eigenvalue spectrum of the improved staggered  $M$ , which will become closer and closer as  $a \rightarrow 0$ . This has been demonstrated numerically (Follana *et al.* 2004) and justifies ‘dividing by 4’ by taking  $(\det M)^{1/4}$  in the path integral to include one quark flavour. The improvement of the staggered quark action to remove the leading-order taste-changing interactions of Figure 10 is done by replacing the gluon fields that appear in the finite difference of Equation 33 with a combination of gluon fields that remove the coupling between the quark and a single  $p = \pi/a$  gluon. The combination ‘smears’ out the gluon field in directions perpendicular to its link by including in combination with a single  $U_\mu(x)$  paths such as ‘the staple’,  $U_\nu(x)U_\mu(x + 1_\nu)U_\nu^\dagger(x + 1_\mu)$ . The simplest improved staggered action with  $a^2$  errors removed uses paths up to those containing 7  $U$  fields in all 3 directions perpendicular to a given link with tadpole-improvement. It is called the asqtad action and has been successfully used in extensive unquenched simulations as described in section 3 on results (Lepage 1998b, Orginos *et al.* 1999).

All quark formulations must give the same physical results in the continuum  $a \rightarrow 0$  limit and this can be usefully checked in the quenched approximation. Figure 11 shows results for the mass of a vector light meson (a ‘ $\rho$ ’) at an arbitrary fixed physical quark mass as a function of lattice spacing (Davies *et al.* 2005). Both axes are given in units of  $r_1$ , defined in a similar way to  $r_0$ , but  $r_1 \approx 0.35\text{fm}$ . The  $x$  axis is in terms of the squared lattice spacing since most of the formalisms plotted have discretisation errors at  $\mathcal{O}(a^2)$  or better. The Wilson formalism, with errors at  $\mathcal{O}(a)$ , is clearly much worse than the other formalisms on this plot, with a very steep  $a$  dependence, but it does give a consistent continuum limit.

Heavy quarks ( $b$  and  $c$ ) represent a rather different set of issues to those for light quarks in lattice QCD. They have large quark masses,  $m_Q$ , and therefore large values of  $m_Q a$  at any value of  $a$  at which we are able to do QCD simulations. This means that we risk large discretisation errors when handling these quarks if we use a formalism in which the errors are set by the size of  $ma$ . If  $m_Q a > 1$  then no amount of improvement will give a good discretisation for these quarks. This is particularly true for the  $b$  quark which has a mass of around 5 GeV. To reduce  $m_Q a$  below 1 requires  $a^{-1} > 5$  GeV or a lattice spacing  $< 0.04$  fm which is incredibly expensive to simulate (as well as being wasteful). Luckily physical understanding of these systems comes to our rescue here. The experimental spectrum of hadrons containing  $b$  and  $c$  quarks shows clearly that the masses of these hadrons are much larger than the differences in mass between the hadrons in different radial and orbital excitations (and these differences are in fact very similar for  $b$  and  $c$  systems). The differences reflect typical kinetic energies and momenta inside the hadrons of a few hundred MeV to a GeV, *ie* of the same size or somewhat larger than those typically inside light hadrons but  $\ll m_Q$ . The quark mass itself is not important for the dynamics of the bound state but simply provides an overall mass shift (Davies 1998). If we formulate the quark action in a way that simulates accurately nonrelativistic quark momenta and kinetic energies we will be able to accurately determine the properties of the hadrons and it is these scales that will also control the discretisation errors.

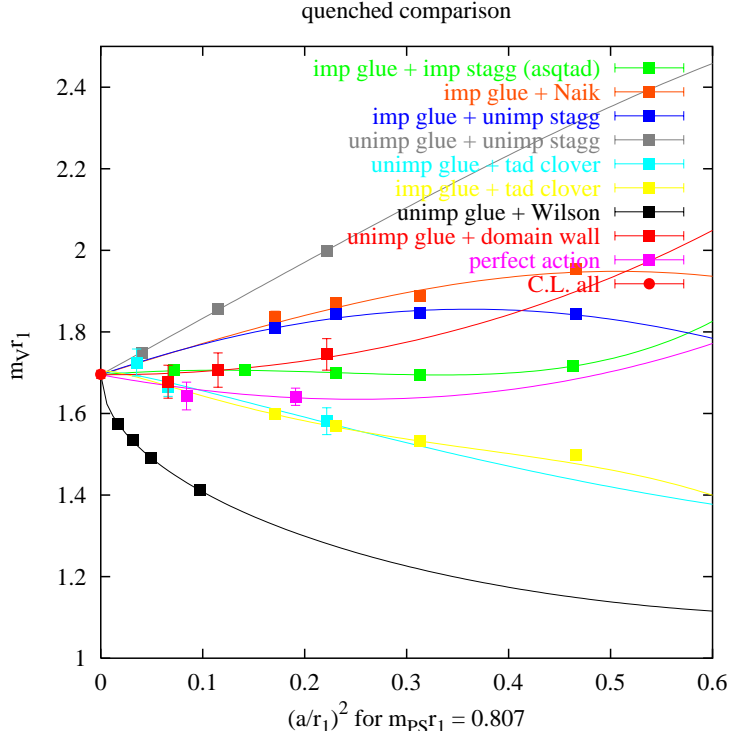


**Figure 11.** Results for the vector light meson mass at fixed physical quark mass in quenched lattice QCD using a variety of gluon and quark actions (for the valence quarks). The mass is given in units of  $r_1$  and plotted as a function of  $a^2$ , also in units of  $r_1$ . The lines represent fits to the lattice results, including appropriate discretisation errors for each case, that require all lines to have a common continuum limit. A good fit is obtained (Davies *et al.* 2005).

This means using a nonrelativistic effective field theory and the example we give here is Nonrelativistic QCD, NRQCD. The lattice NRQCD action is a discretised nonrelativistic expansion of the Dirac action, matched to continuum QCD to the desired order in the heavy quark velocity,  $v_Q$  and in the strong coupling constant,  $\alpha_s$  (Lepage *et al.* 1992). The first few terms of the continuum NRQCD quark Lagrangian are:

$$\mathcal{L}_Q = \bar{\psi} \left( D_t - \frac{\vec{D}^2}{2m_Q} - c_4 \frac{\vec{\sigma} \cdot \vec{B}}{2m_Q} + \dots \right) \psi \quad (34)$$

where we include just the non-relativistic kinetic energy term and the coupling between the quark spin and chromomagnetic field. Higher order terms give the spin-orbit interaction and Darwin term *etc.*  $\psi$  is a 2-component spinor here but the antiquark Lagrangian is simply related to the quark one and so the antiquark propagator is easily determined without a separate calculation. On the lattice the covariant time and space derivatives above become finite differences with  $U$  fields included. The presence of a single time derivative means that the calculation of the quark propagator,  $M^{-1}$ , can be solved as an

initial value problem on one pass through the lattice. This is much faster than the iterative methods needed for light quarks. On the lattice  $m_Q$  becomes  $m_Q a$ , the quark mass in lattice units, and this must be determined by getting a heavy hadron mass correct, for example the  $\Upsilon$  mass. This is slightly more complicated than in the light quark mass case because the direct mass term is missing from the Lagrangian, so the energy exponent of an  $\Upsilon$  correlator at zero momentum will not give the mass (although energy differences do give mass differences). Instead we have to calculate hadron energies at non-zero spatial momentum and extract the mass of the hadron from its kinetic energy.

NRQCD contains, by design, the low momentum physics of QCD for heavy quarks. High-momentum interactions of continuum QCD are missing, and the lattice in any case does not allow for  $p > \pi/a$ . The effect of these missing high-momentum interactions is included in NRQCD through a renormalisation of the coefficients,  $c_i$ , of the higher order terms. Because the effects that we are talking about are high momentum, the calculation can be done in perturbation theory as a powers series in  $\alpha_s$ . Again small deviations from 1 are found after tadpole-improvement of the  $U$  fields is implemented, provided  $m_Q a$  is not large. The  $c_i$  contain functions of  $m_Q a$ , including inverse powers of  $m_Q a$ , multiplying powers of  $\alpha_s$  and so we cannot take  $a$  to zero or we lose control of the convergence of the  $c_i$ . This is not a problem in practice since, as discussed earlier, discretisation errors can now be controlled in this formalism to high accuracy at values of the lattice spacing that we can simulate and there is no need to take  $a$  very small.

For charm quarks the situation is not as clear as for  $b$  quarks because  $m_c a \approx 1$  on lattices in current use. NRQCD does not necessarily work well and it may be more advantageous to take a relativistic formalism of the  $c$  quark and attempt to improve it highly to reduce the discretisation errors in  $m_c a$  to a reasonable level. The Fermilab formalism does a mixture of both these things by using a relativistic action, the clover action, but interpreting it non-relativistically where necessary to avoid the largest discretisation errors (El-Khadra *et al.* 1997). This is the method currently being used most extensively for  $c$  quarks and results will be described in section 3. Another promising method is to use anisotropic lattices in which the lattice spacing in the time direction is much finer than that in spatial directions. This then allows  $m_c a_t$  to be small without requiring a huge amount of computer power to make a fine grid in 4-dimensions. The price of this is a relatively complicated action, however.

### 3 Results

Recent lattice results which include for the first time realistic quark vacuum polarisation effects, have changed the landscape of lattice calculations. We will concentrate on those results here and the possibilities for the future that they engender.

The new results are based on gluon field configurations generated by the MILC collaboration and analysis by the HPQCD and MILC collaborations (Davies *et al.* 2004). They have worked with a highly improved gluon action and with improved staggered (asqtad) quarks, as described in the previous section. The effect of the quark vacuum polarisation is included in the generation of the gluon configurations by taking the fourth root of the determinant of the improved staggered quark matrix for each flavour of quark included in the sea. Three flavours of quarks are included in the sea,  $u$ ,  $d$  and  $s$ . This is

believed to be all that is necessary, since a perturbative analysis shows that the effects of  $c$  or  $b$  quarks in the sea is very small (Nobes 2005). The  $u$  and  $d$  quarks are taken in fact to have the same mass (as in all current lattice calculations) because this provides for some simplification and should give only a small error when comparison is made to appropriately isospin-averaged experimental quantities. The configurations are then referred to as ‘2+1’ flavour unquenched configurations.

As described above, it is not possible to perform the lattice calculations at the physical  $u/d$  quark mass (since we take  $m_u = m_d$  this would be  $(m_{u,phys} + m_{d,phys})/2$ ). Instead, many different ensembles of configurations are made with different values of  $m_{u/d}$  and extrapolations to find the physical point must be done. These chiral extrapolations will be accurate provided that we are close enough to the physical point and we are able to constrain the functional form of the dependence on  $m_{u/d}$  with chiral perturbation theory.

It is convenient, when discussing the  $u/d$  quark masses used in the lattice calculations, to give them in terms of the strange quark mass,  $m_s$ . This is because there is no problem (with current computers) in doing lattice QCD calculations that include the  $s$  quark vacuum polarisation. However, it is also clear that, in the real world, there is a very visible difference between  $s$  quarks and  $u/d$  quarks. Indeed, if we consider chiral perturbation theory as an expansion in powers of  $x_q = (m_{PS}/(4\pi f_\pi))^2$  where  $m_{PS}$  is the mass of the pseudoscalar light meson made from the light quarks, then  $x_s = 0.33$  and  $x_{u/d} = 0.03$ . We would therefore not expect low order chiral perturbation theory to work well for light quarks with a mass equal to that of the  $s$  quark. This is not a problem since we do not need chiral perturbation theory to reach the  $s$  quark mass. However it does mean that our  $u/d$  quark mass must be well below  $m_s$  to expect to be able to reach the physical point by chiral extrapolation in  $m_{u/d}$ . However, with a set of ensembles with  $m_{u/d} < m_s/2$  and using next-to-leading order chiral perturbation theory in  $m_{u/d}$ , it should be possible to perform extrapolations with errors at the few % level. This is what has now been done using the configurations generated by the MILC collaboration. The MILC configurations range in  $m_{u/d}$  down to  $m_{u/d} = m_s/8$  which is within a factor of three of the real world. This is a huge improvement over previous calculations which had only two flavours of sea quarks, meant to represent  $u$  and  $d$ , but with  $m_{u/d} > m_s/2$ , and it is this improvement that is responsible for the quality of the new results.

In addition to including the effect of quark vacuum polarisation with light  $u/d$  quarks and  $s$  quarks, the MILC configurations come in sets with three different values of the lattice spacing. In each set the bare coupling constant must be adjusted as the quark masses are changed to keep the lattice spacing approximately the same (as described earlier the lattice spacing is determined accurately after the simulation, but preliminary results enable this approximate tuning of the lattice spacing to be done). Having a set of configurations which include the effect of sea quarks of different light quark mass but which have the same lattice spacing is important to allow the chiral extrapolations to be done without confusing the (real) effects of changing  $m_{u/d}$  with (unphysical) systematic errors from having different values of the lattice spacing. The effect of the discretisation errors can also be gauged accurately (and an extrapolation to the continuum limit be performed if necessary) by having several well-spaced values of the lattice spacing. Again this has not been possible with previous lattice calculations. On the MILC configurations the lattice spacing values are approximately 0.18 fm (supercoarse), 0.12 fm (coarse) and 0.08fm (fine), chosen to be appropriately spaced in  $a^2$ , the expected size of the discretisation er-

rors with the improved action used. Most of the results described here will come from the coarse and fine sets, since the supercoarse set has only been made recently. A superfine set is also now planned, to give a fourth lattice spacing value. In addition another set of ensembles is being made with a different bare sea  $s$  quark mass. There is no problem in principle with working at the correct  $s$  mass, but it is hard to tune this accurately until after the calculations have been done. On the coarse ensemble the sea  $s$  mass is in fact 25% high and it is 10% high on the fine set of ensembles. Results with a different  $s$  mass will enable a more accurate interpolation to the correct  $s$  mass.

Whilst singing the praises of the MILC configurations, it should also be said that they have a commendably large volume (2.5 fm on a spatial side) and a very long extent in the time direction (nearly 8 fm). There are several hundred configurations in each ensemble that can be used for calculations. All of these factors lead to small statistical errors, indeed smaller than for a lot of calculations that have been done in the quenched approximation. The MILC configurations are publicly available at [www.nersc.gov](http://www.nersc.gov).

### 3.1 Results on the spectrum

Figure 12 summarises the new results (Davies *et al.* 2004). It shows the ratio of the lattice calculation to the experimental number for a range of gold-plated quantities from the  $\pi$  decay constant to radial and orbital excitation energies in the  $\Upsilon$  system, by way of heavy-light meson masses and baryon masses. The left-hand panel of the Figure shows results in the old quenched approximation and the right-hand panel shows the new results including the effect of light quark vacuum polarisation. The clear qualitative difference between the two panels is that the left-hand panel shows clear disagreement with experiment for a number of quantities because the quenched approximation is wrong. The right-hand panel shows instead agreement with experiment for all the quantities within errors of a few percent.

To make Figure 12 the parameters of QCD first had to be fixed. The lattice spacing was determined from the radial excitation energy in the  $\Upsilon$  system ( $2S - 1S \equiv M_{\Upsilon'} - M_{\Upsilon}$ ). The  $u/d$  quark mass was fixed by finding where the  $\pi$  mass would be correct by extrapolation using chiral perturbation theory. The  $s$  quark mass was fixed by determining where the  $K$  meson mass was correct. The  $c$  quark mass was fixed using the  $D_s$  and the  $b$  quark mass was fixed by getting the  $\Upsilon$  mass correct. All of the hadron masses used to determine the parameters are ‘gold-plated’ *ie* they have very small decay widths and are well below strong decay thresholds. This means that they are well-defined experimentally and theoretically and should be accurately calculable in lattice QCD. Using them to fix parameters will not then introduce unnecessary additional systematic errors into lattice results for other quantities. This is an important issue when lattice QCD is to be used as a precision calculational tool.

Having fixed the parameters, we can then focus on other gold-plated masses and decay constants and Figure 12 shows the predictions for these other quantities. The fact that the right-hand panel demonstrates agreement with experiment for all the quantities shown is an indication that the parameters of QCD are unique. Instead of using the hadron masses of the previous paragraph to fix the parameters we could have used appropriate quantities from Figure 12 and we would have obtained the same answer (and would then have been able to predict  $m_{\pi}$ ,  $m_K$  etc). The left-hand panel shows that this is not true in

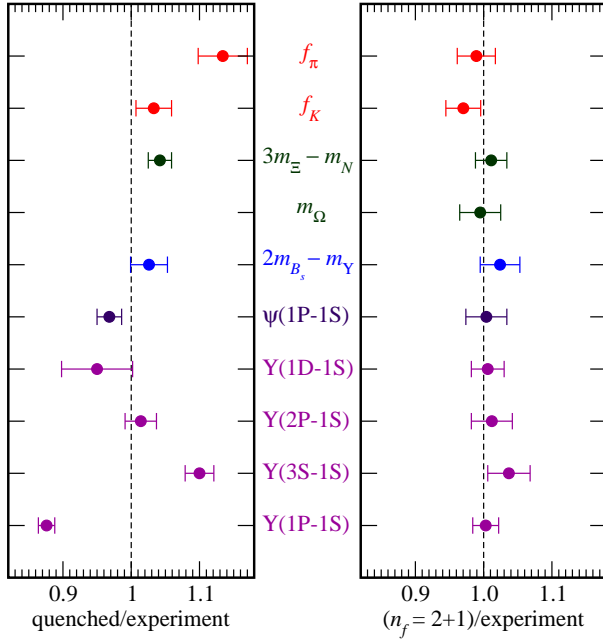


**Figure 12.** Lattice QCD divided by experiment for a range of ‘gold-plated’ quantities that cover the full range of QCD physics. The unquenched calculations on the right show agreement with experiment across the board, whereas the quenched approximation on the left gives systematic errors of  $\mathcal{O}(10\%)$ . (Davies *et al.* 2004)

the quenched approximation. The results there show disagreement with experiment and it is clear, for example, that if we had used the orbital excitation energy in the  $\Upsilon$  system ( $1P - 1S$ ) to fix the lattice spacing we would have obtained an answer 10% different. The quenched approximation is then internally inconsistent since the parameters depend on the hadrons used to fix them. The basic reason is that, as the light quark vacuum polarisation is missing, the strong coupling constant runs incorrectly between different momentum scales. Therefore hadrons which are sensitive to different momentum scales cannot simultaneously agree with experiment.

In Figure 13 more details are shown of the lattice results for the radial and orbital energy levels in the  $\Upsilon$  system in the old quenched approximation and now using the MILC configurations with their inclusion of a realistic light quark vacuum polarisation (Gray *et al.* 2003). Our physical understanding of the  $\Upsilon$  system is very good and there are a lot of gold-plated states below decay threshold so it is a very valuable system for lattice QCD tests and for determining the lattice spacing. We use the standard lattice NRQCD effective theory, described above, for the valence  $b$  quarks, accurate through  $v^4$  where  $v$  is the velocity of the  $b$  quark in its bound state. This means that spin-independent splittings, such as radial and orbital excitations, are simulated through next-to-leading-order and should be accurate to about 1%. The test of QCD using these splittings is then a very accurate one. We do not expect the  $\Upsilon$  system to be very sensitive to the masses of the light quarks included in the quark vacuum polarisation, only to their number. The



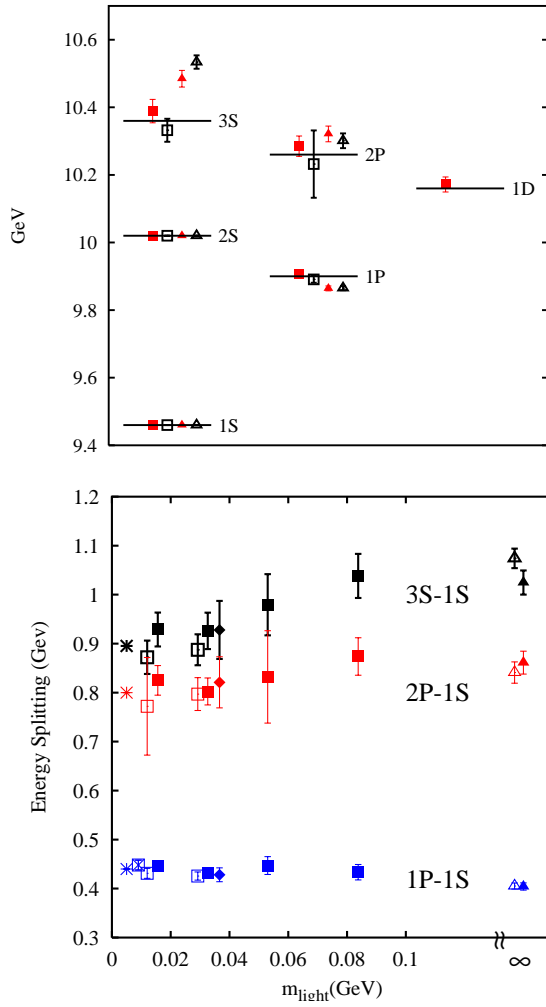


**Figure 13.** Radial and orbital splittings in the  $\Upsilon$  spectrum from lattice QCD in the quenched approximation and including a realistic light quark vacuum polarisation. In these plots the  $b$  quark mass was fixed from the  $\Upsilon$  mass and the lattice spacing from the splitting between the  $\Upsilon'$  and the  $\Upsilon$ . Neither of these masses is predicted. (Top) The spectrum of S, P and D levels in the  $\Upsilon$  system obtained from coarse (filled red triangles) and fine (open black triangles) quenched lattice calculations and from coarse (filled red squares) and fine (open black squares) unquenched calculations. Experimental results are shown as lines. (Bottom) Results for different splittings as a function of light  $u/d$  quark mass. The leftmost points, at lightest  $u/d$  quark mass, are the ones included in the top plot for the unquenched results. (Gray et al. 2003)

momentum transfer inside an  $\Upsilon$  is larger than any of the  $u$ ,  $d$ , or  $s$  masses and so we expect these splittings simply to ‘count’ the presence of the light quarks. This lack of variation with light quark mass is evident in Figure 13.

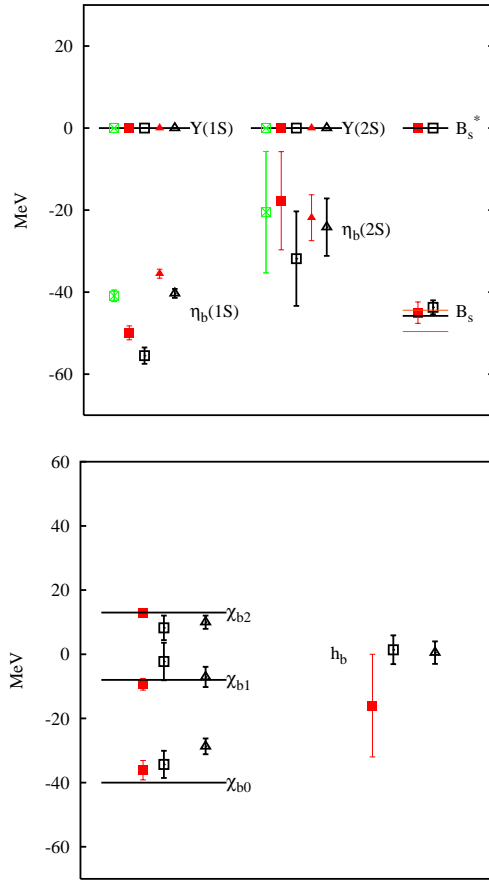


**Figure 14.** Fine structure in the  $\Upsilon$  system. Triangles show quenched results (closed red=coarse, open black=fine) and squares show unquenched results (crossed green=supercoarse, closed red=coarse, open black=fine). (Top)  $S$ -wave splittings between  $\Upsilon$  and  $\eta_b$  and between  $\Upsilon'$  and  $\eta_b'$ . The same NRQCD action is used to determine the splitting between the  $B_s^*$  and the  $B_s$  and this is shown on the right. There the experimental situation is summarised by the lines - faint lines show limits for the experimental  $B_s$  results, the darker line shows the more precise result for the  $B$ , which is expected to be very close to the result for the  $B_s$ . (Bottom)  $P$ -wave splittings between the  $^3P_{0,1,2}$   $\chi_b$  states, compared to experiment. The results on the right show the lattice prediction for the unseen  $^1P_1$   $h_b$  state. (Gray et al. 2003)

Figure 14 shows the fine structure in the  $\Upsilon$  spectrum. Since the fine structure is determined at leading order by spin-dependent terms that appear first at  $\mathcal{O}(v^4)$  this has significant systematic errors from missing higher order terms. There are also systematic errors arising from missing radiative corrections to the leading  $v^4$  terms. In fact, encouraging agreement with experiment is obtained and we are able to predict the ground-state hyperfine splitting between the  $\Upsilon$  and the unseen  $\eta_b$  to be 60(15) MeV. The results for

the fine structure can be improved by improving the NRQCD action and this will be done in the near future. For comparison to the  $\Upsilon$  splittings, Figure 14 also shows the splitting between corresponding mesons made of one  $b$  quark and one  $s$  quark *ie* the  $B_s$  heavy-light system. This is calculated on the lattice using the same NRQCD action of the valence  $b$  quarks and the improved staggered action (as used in the quark vacuum polarisation) for the light quark. Once the  $b$  quark mass and lattice spacing have been fixed from the  $\Upsilon$  system the heavy-light spectrum is entirely predicted by lattice QCD and provides another useful test against experiment.

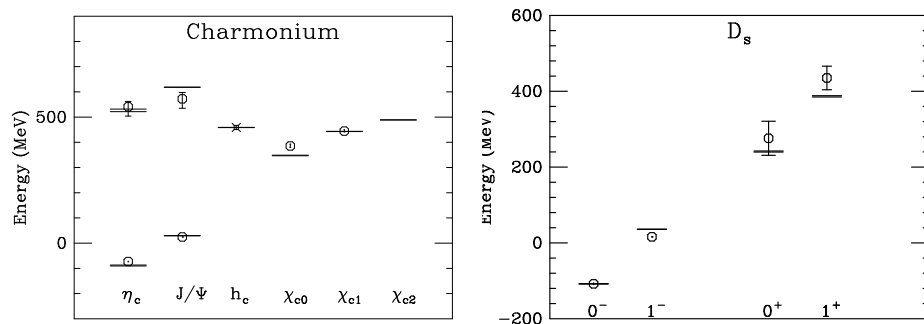


**Figure 15.** Spectrum of mesons containing charm quarks from lattice QCD including light quark vacuum polarisation. These results are from the coarse unquenched MILC configurations using the  $\Upsilon$  system to determine the lattice spacing and the  $D_s$  meson mass to fix the  $c$  quark mass. The Fermilab action was used for the  $c$  quark. (Left) The charmonium system. (Right) The  $D_s$  system. (di Pierro *et al.* 2004)

The charm quark is somewhat too light for good results using the NRQCD action above. The results shown in Figure 15 use the Fermilab action described earlier which aims to interpolate between light relativistic quarks and the heavy nonrelativistic limit (di Pierro *et al.* 2004). It should be borne in mind that there are fewer gold-plated states in the  $c\bar{c}$  spectrum compared to the  $b\bar{b}$  spectrum described above. In fact even the  $\psi'$  is rather close to decay threshold to be sure that its mass is not affected by coupling to virtual decay modes which will have a distorted momentum spectrum on a finite lattice volume. The right-hand plot of Figure 15 shows the  $D_s$  spectrum. The  $D_s$  mass was used to fix the  $c$  quark mass, so that is not predicted. The two newly discovered  $0^+$  and  $1^+$  states are shown. The simplest explanation for these states is that they are  $P$ -wave states, narrow because their masses are too low for the Zweig-allowed decay to  $D, K$ . They do decay to  $D_s, \pi$ , however, and are therefore not gold-plated. We expect systematic errors in a lattice QCD calculation of their masses, even when light quark vacuum polarisation is included. The current lattice results, shown in Figure 15, are consistent with this picture and certainly do not require any more exotic explanation of the meson internal structure.

With a good action for  $b$  quarks and a good action for  $c$  quarks it is possible to predict the mass of the  $B_c$  meson. The results are shown in Figure 16, (Allison *et al.* 2005) compared to the very recent experimental results (Acosta *et al.* 2005). The quantity that is calculated on the lattice is the mass difference between the  $B_c$  and a combination of masses of other mesons containing a  $b$  quark and a  $c$  quark, enabling some of the sys-

tematic errors to cancel. There are two combinations available on the lattice. The one that gives the most accurate result we believe is to calculate the difference between the  $B_c$  mass and that of the average of the  $\Upsilon$  and  $\psi$ . This is called  $\Delta_{\psi\Upsilon}$ . It turns out to be very small, although non-zero. The difference between the  $B_c$  and the sum of the masses of the  $D_s$  and  $B_s$ ,  $\Delta_{D_s B_s}$ , is also useful but less accurate. Both splittings are shown in Figure 16 as a function of the light quark mass included in the quark vacuum polarisation on the MILC unquenched configurations. After a study of systematic errors from fixing the quark masses and lattice spacing we are able to give a final result for the  $B_c$  mass of 6304(20) MeV (Allison *et al.* 2005). The error is much better than the 100 MeV obtained for previous calculations in the quenched approximation. There 100 MeV arose directly from the impossibility of consistently determining the parameters of the theory in the quenched approximation, a problem that disappears in the new unquenched results. The very recent experimental result from CDF is 6287(5) MeV, showing impressive agreement with the unquenched lattice calculation (Acosta *et al.* 2005).

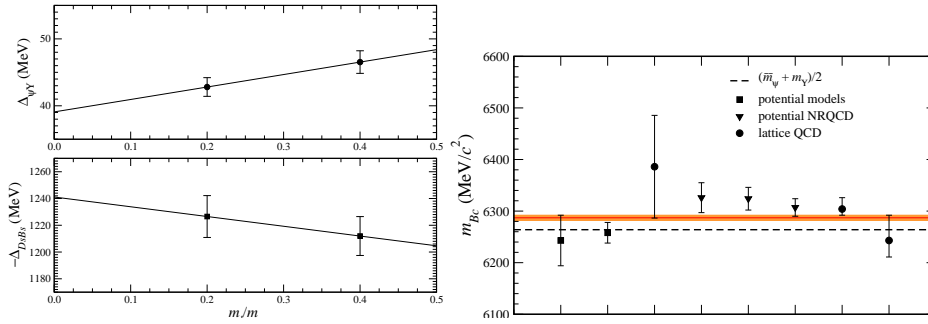


**Figure 16.** (Left) The differences between the  $B_c$  mass and, above, the average of  $\Upsilon$  and  $\psi$  masses and, below, the  $B_s$  and  $D_s$  masses, plotted against the light quark mass included in the quark vacuum polarisation in the MILC unquenched configurations. (Right) Predictions for the mass of the  $B_c$  from a variety of methods. In the centre is the old quenched lattice QCD result and on the right the two new lattice QCD predictions. The dashed line shows where the  $B_c$  mass would be equal to the average of  $\Upsilon$  and  $\psi$  masses and the broader coloured line is the new experimental result. (Allison *et al.* 2005, Acosta *et al.* 2005)

Results for light mesons are equally good on the MILC configurations (Aubin *et al.* 2004a, 2004b, Bernard 2001). Figure 17 shows results for the light meson masses and decay constants plotted against light quark mass. The left-hand plot shows the fits to chiral perturbation theory for the squared masses of the  $\pi$  and  $K$ , which must then be extrapolated (for the  $\pi$ ) or interpolated (for the  $K$ ) to find the quark masses which correspond to  $u/d$  (bearing in mind that the  $u$  and  $d$  quark masses have been taken to be the same) and  $s$ . Once this has been done, predictions for other light meson quantities can be made. Two very clean quantities to calculate are the light meson decay constants,  $f_\pi$  or  $f_K$ . The decay constant is obtained from the matrix element of the temporal axial current between the pseudoscalar light meson and the QCD vacuum and it is related, for the charged  $\pi$  and  $K$ , to the rate of purely leptonic decay. This rate is well-known experimentally for these mesons and can be calculated accurately on the lattice. This is because, unlike the matrix elements we will discuss below, the axial current needs no

renormalisation for improved staggered quarks. The right-hand plot of Figure 17 shows the chiral extrapolations for the  $\pi$  and  $K$  decay constants for the fine MILC lattices. Only points for which the  $u/d$  quark mass is less than half the  $s$  quark mass are used in the fits to chiral perturbation theory. The curves, however, show what happens when these fits are extrapolated to higher  $u/d$  quark masses. For  $f_\pi$  it is clear that the heavier  $u/d$  quark are not on the same chiral perturbation theory curve as the lighter ones *ie* using heavier  $u/d$  masses would have distorted the chiral fit and given the wrong result in the chiral limit where the  $u/d$  quark mass takes the correct value to give the experimental  $\pi$  meson mass. This should be borne in mind when looking at earlier lattice results that have only  $m_{u/d} > m_s/2$ .

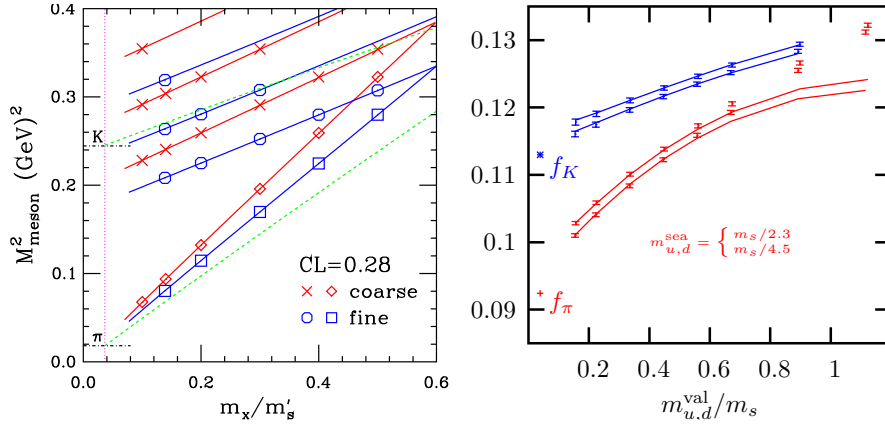


**Figure 17.** (Left) Chiral fits and extrapolations for light meson ( $\pi$  and  $K$ ) meson masses from the MILC configurations. The square of the meson mass is plotted against the light ( $u/d$ ) quark mass used in the quark vacuum polarisation. This is denoted  $m_x$  and given in units of the  $s$  quark mass used in the quark vacuum polarisation (denoted here  $m'_s$ ). Several different values of valence  $s$  quark mass were used so there are several different sets of results for the  $K$  mass. The lattice results are the points and lines are high-order chiral perturbation theory fits. At small light quark mass these are indistinguishable from the lowest order straight line. (Right) Chiral fits for  $f_\pi$  and  $f_K$ , the  $\pi$  and  $K$  decay constants. The points are lattice calculations on the fine unquenched MILC configurations, for two different values of the light quark mass in the quark vacuum polarisation ( $m_{u/d}^{\text{sea}}$ ). The results are plotted against the valence  $u/d$  quark mass in units of the valence  $s$  quark mass. Note that only points with  $m_{u/d} < m_s/2$  (for both valence and sea) were used in the chiral fits, shown as lines. The fits were then extrapolated back to compare to the lattice results with  $m_{u/d}^{\text{valence}} > m_s/2$ . (Aubin *et al.* 2004a, 2004b, Lepage and Davies 2004)

Light baryons are also gold-plated particles and calculating their masses provides a further opportunity for predictions from lattice QCD since all the QCD parameters have been fixed from the meson sector. Baryons are harder to work with on the lattice and the masses are not as precise. The nucleon also requires, for example, a more complicated chiral fit and this has not yet been done. Figure 18 shows the nucleon results on the super-coarse, coarse and fine MILC unquenched configurations (Aubin *et al.* 2004a).

There are signs that the results change slightly with lattice spacing *ie* there is a visible discretisation error. This needs to be studied further. The line shows the low order chiral perturbation theory result and the lattice results do seem to be heading towards that on the finer lattices. The right-hand plot shows results for the  $\Omega$  baryon made of three valence  $s$  quarks (Toussaint and Davies 2005). This baryon is not very dependent on the  $u/d$  quark mass used in the quark vacuum polarisation so chiral extrapolations are much simpler. Its mass is sensitive to the  $s$  quark mass, however, so the fact that agreement with the experimental result is obtained with the  $s$  quark mass fixed from the  $K$  is another strong confirmation that lattice QCD is internally consistent once realistic quark vacuum polarisation is included.

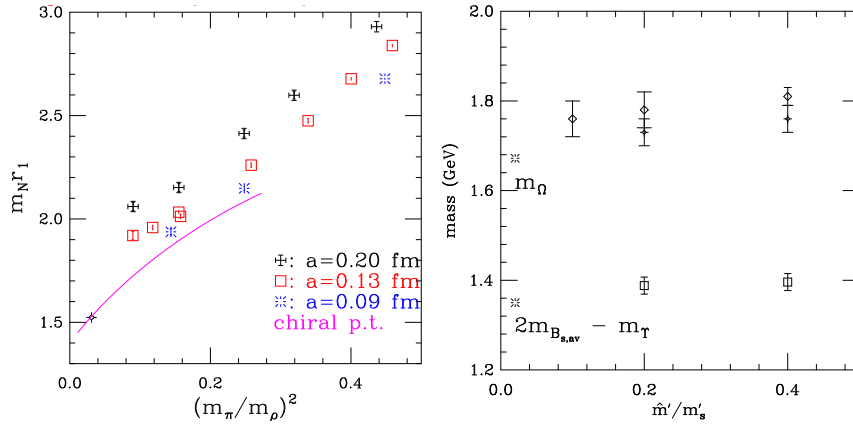


**Figure 18.** (Left) The nucleon mass in units of the  $r_1$  parameter from the unquenched MILC configurations at three different values of the lattice spacing and for several values of the light quark mass, denoted on the  $x$  axis by the ratio of  $\pi$  to  $\rho$  masses made of the light quarks. The line shows continuum chiral perturbation theory for this quantity (Aubin et al. 2004a). The fancy diamond gives the experimental point in these units. (Right) The  $\Omega$  baryon mass as a function of sea light quark mass  $m'$  divided by sea  $s$  quark mass. The  $\Omega$  mass is calculated for a valence  $s$  quark mass which is the correct one, fixed from the  $K$  (Toussaint and Davies 2005). The burst gives the experimental point. Also on this plot is the splitting between the spin average of the  $B_s$  and  $B_s^*$  and the  $\Upsilon$ , a quantity sensitive to the  $s$  quark mass, but not the  $b$  quark mass. Again it shows good agreement with experiment denoted by a burst (Aubin et al. 2004c).

It is important to realise that accurate lattice QCD results are not going to be obtainable in the near future for every hadronic quantity of interest. What these results show is that ‘gold-plated’ quantities should now be calculable. Unstable hadrons, or even those within 100 MeV or so of Zweig-allowed decay thresholds, have strong coupling to their real or virtual decay channel and this is not correctly simulated on the lattice volumes currently being used. *eg* the smallest non-zero momentum on typical current lattices exceeds 400 MeV. This could significantly distort the decay channel contribution to the hadron mass. Much larger volumes will then be necessary to handle these hadrons. Unfortunately the list of non-gold-plated hadrons is a long one - it includes the  $\rho$ ,  $\phi$ ,  $D^*$ ,  $\Delta$ ,  $N^*$ , glueballs, hybrids *etc.* Some of these may be more accurately calculable than others and qualitative results may also be useful. These points must be borne in mind,

however, when making quantitative comparison between lattice QCD and experiment.

### 3.2 Determination of the parameters of QCD

Lattice QCD calculations are an excellent way to determine the parameters of QCD, masses and coupling constant, because the method is a very direct one.

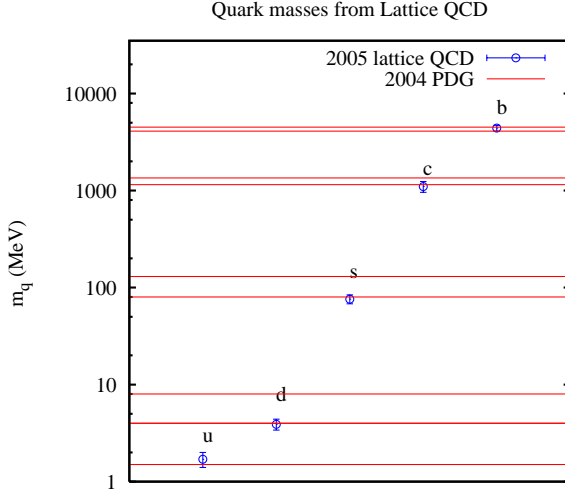


**Figure 19.** Quark masses in the  $\overline{MS}$  scheme at a relevant scale (2 GeV for  $u$ ,  $d$  and  $s$  and their own mass for  $c$  and  $b$ ) as determined from lattice QCD using the unquenched MILC configurations (Aubin *et al.* 2004c, 2004b, Gray *et al.* 2003, Nobes *et al.* 2005). The lines give the range of the current values quoted in the Particle Data Tables (PDG 2004).

For the quark masses we directly determine the bare quark masses in the lattice QCD Lagrangian required to give the correct answer for a given hadron mass. With the inclusion of light quark vacuum polarisation we have seen above that this can be done both accurately and unambiguously. Masses are more conventionally quoted in the continuum  $\overline{MS}$  renormalisation scheme rather than the lattice scheme. To convert from the lattice scheme to  $\overline{MS}$  requires the calculation of a finite renormalisation factor to take into account the gluon radiation with momenta larger than  $\pi/a$  that does not exist on the lattice. The renormalisation factor can be calculated in perturbation theory since it involves large momenta, and it then appears as a power series in  $\alpha_s$ . This calculation has been done to  $\mathcal{O}(\alpha_s)$  for the light quark masses for the improved staggered quark action (Hein *et al.* 2003). The  $u/d$  quark mass was fixed from  $m_\pi$  and the  $s$  quark mass from  $m_K$  as described above. They were then converted to the  $\overline{MS}$  scheme using the renormalisation factor. This gave, quoting the masses at the conventional scale:

$$\begin{aligned} m_s^{\overline{MS}}(2\text{GeV}) &= 76(8)\text{MeV}, \\ m_{u/d}^{\overline{MS}}(2\text{GeV}) &= 2.8(3)\text{MeV}, \end{aligned} \quad (35)$$

where  $m_{u/d}$  is the average of  $u$  and  $d$  masses (Aubin *et al.* 2004c). The main source of error from the lattice calculation is from unknown higher order terms in the perturbative renormalisation factor to convert to  $\overline{MS}$ . A two-loop calculation will be available shortly and this will reduce the error to a few %. This is a huge improvement over previous determinations of the masses from *eg* QCD sum rules. Figure 19 shows the results for all 5 quark masses ( $u$  and  $d$  are determined separately by matching to different combinations of charged and neutral pions and kaons) obtained on the MILC configurations and using 1-loop matching to convert to the conventional  $\overline{MS}$  scheme, compared to the results from the 2004 Particle Data Tables (PDG 2004). It is quite clear that the lattice will take the lead in providing accurate quark masses now.

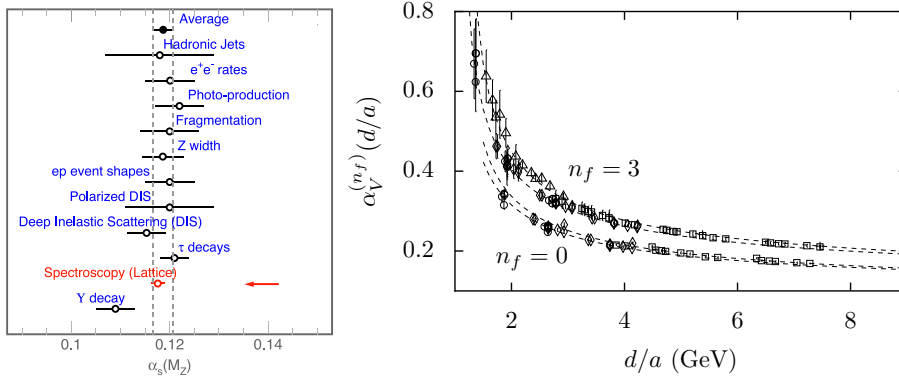


**Figure 20.** (Left) A comparison of the new lattice determination of  $\alpha_s$ ,  $0.1170(12)$  with the results from other determinations in the Particle Data Tables (PDG 2004). (Right) The determination of  $\alpha_s$  from the lattice in the  $V$  scheme on quenched ( $n_f = 0$ ) and unquenched ( $n_f = 3$ ) gluon configurations at various energy scales,  $d/a$  for a variety of Wilson loop operators. The dashed curves show the expected running of  $\alpha_s$  in the two cases from QCD. (Mason *et al.* 2005)

The strong coupling constant,  $\alpha_s$ , is also well-determined on the lattice (Mason *et al.* 2005). The determination of  $\alpha_s$  proceeds by the calculation in perturbation theory to high order of some lattice operator (Trottier 2004). Recently calculations up to and including terms in  $\alpha_s^3$  became available for a lot of different Wilson loops and combinations of them. These could then be readily ‘measured’ (*ie* calculated) on the MILC configurations. From each non-perturbative lattice calculation compared to perturbation theory a value for  $\alpha_s$  is extracted at some momentum scale in lattice units. From the determination of the lattice spacing, this scale can then be converted to a physical scale in GeV and  $\alpha_s$  evolved to different scales use the QCD  $\beta$  function. Because results at three different values of the lattice spacing are available, it is possible to do a consistency check for the determination of  $\alpha_s$  at a given physical scale from three different determinations of a particular Wilson loop at three different lattice scales. This allows estimates of fourth order terms in the perturbation theory, which puts this calculation into a new regime of accuracy for  $\alpha_s$  determinations. Altogether 28 different loops and loop combinations were studied. The  $\alpha_s$  determined was converted to the  $\overline{MS}$  scheme and run to the scale of  $M_Z$  since again this is the conventional comparison point. The final answer obtained is  $0.1170(12)$  which compares very well with other determinations quoted in the Particle



Data Tables, see Figure 20.

Another interesting point is that  $\alpha_s$  is well able to distinguish between quenched and unquenched configurations. Figure 20 shows corresponding determinations of  $\alpha_s$  from MILC quenched and unquenched configurations for different Wilson loops. The relevant momentum for the  $\alpha_s$  determination varies from loop to loop and also depends on whether the result comes from the super-coarse, coarse or fine lattices. This enables a comparison of  $\alpha_s$  values with the expected curve for the running. The agreement is very good and shows both that the quenched ( $n_f=0$ ) and unquenched ( $n_f=3$ )  $\alpha_s$  figures differ markedly and also run differently, both in agreement with the perturbative expectation (Mason *et al.* 2005).

### 3.3 Results on matrix elements

A key point where lattice QCD calculations are needed and can make an impact is in the determination of the elements of the Cabibbo-Kobayashi-Maskawa matrix that links the quark flavours under weak decay in the Standard Model of particle physics. When a quark changes flavour inside a hadron with the emission of a  $W$  the quark level process is quite simple (see Figure 24). However, this decay unavoidably takes places inside a hadron because the quarks are confined by QCD and the QCD corrections to the decay rate are significant. This is why the decay matrix element need to be calculated in lattice QCD so that all of the gluonic radiation around the decay vertex can be taken into account. A CKM element  $V_{f_1 f_2}$  multiplies the vertex but this appears in a simple way in the final theoretical answer for the decay rate since there is only one weak vertex in the process. A comparison of the experimental decay rate and the lattice QCD results times  $V_{f_1 f_2}^2$  then gives  $V_{f_1 f_2}$ .

Decay rates which can be accurately calculated in lattice QCD are those for gold-plated hadrons in which there is at most one (gold-plated) hadron in the final state. This therefore includes leptonic and semi-leptonic decays and the mixing of neutral  $B$  and  $K$  mesons. Luckily there is a gold-plated decay mode available to extract each element (except  $V_{tb}$ ) of the CKM matrix which mixes quark flavours under the weak interactions in the Standard Model:

$$\left( \begin{array}{ccc} \mathbf{V}_{ud} & \mathbf{V}_{us} & \mathbf{V}_{ub} \\ \pi \rightarrow l\nu & K \rightarrow l\nu & B \rightarrow \pi l\nu \\ & K \rightarrow \pi l\nu & \\ \mathbf{V}_{cd} & \mathbf{V}_{cs} & \mathbf{V}_{cb} \\ D \rightarrow l\nu & D_s \rightarrow l\nu & B \rightarrow D l\nu \\ D \rightarrow \pi l\nu & D \rightarrow K l\nu & \\ \mathbf{V}_{td} & \mathbf{V}_{ts} & \mathbf{V}_{tb} \\ \langle B_d | \bar{B}_d \rangle & \langle B_s | \bar{B}_s \rangle & \end{array} \right)$$

The determination of the CKM elements and tests of the self-consistency of the CKM matrix are the current focus for the search for Beyond the Standard Model physics and lattice calculations of these decay rates will be a key factor in the precision with which this can be done.

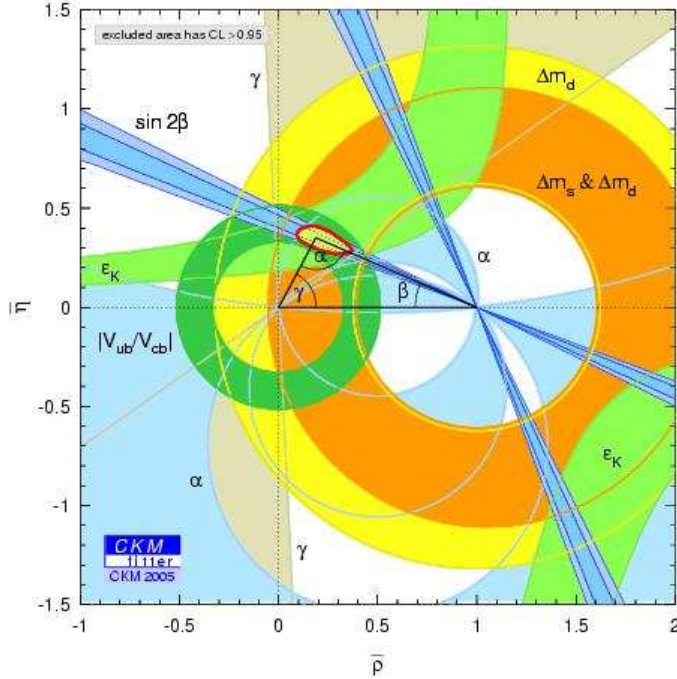


**Figure 21.** Current constraints on the vertex of the ‘unitarity triangle’ made from the Cabibbo-Kobayashi-Maskawa matrix. (CKMfitter 2005)

Figure 21 shows the current ‘unitarity triangle’ picture in which limits are placed on various combinations of elements of the CKM matrix and the result is expressed as a search for the vertex of a triangle. The limits that depend on results from  $B$  factories and the associated lattice calculations, are the dark green ring and the orange and yellow rings. The light green hyperbola comes from kaon physics and associated lattice calculations. The dark green ring is fixed from semileptonic decays of  $B$  mesons to  $\pi$  mesons or  $D$  mesons. The orange and yellow rings result from mixing of neutral  $B$  or  $B_s$  mesons. We will discuss further below the lattice results for these matrix elements. The angles of the unitarity triangle, such as  $\sin(2\beta)$ , are determined directly by the experiment (light blue lines) without theoretical input.

Decay matrix elements of this kind can be calculated on the lattice from the amplitudes of the exponentials in the fit functions for hadron masses, Equation 28. For example, the rate at which a  $B$  meson decays completely to leptons via a  $W$  boson depends on the matrix element of the heavy-light axial vector current,  $J_{A_\mu} = \bar{\psi}_b \gamma_\mu \gamma_5 \psi_u$ , between a  $B$  meson and the (QCD) vacuum. The matrix element of this current is parameterised by the decay constant,  $f_B$ , so that

$$\langle 0 | J_{A_\mu} | B \rangle = p_\mu f_B \quad (36)$$

(using a relativistic normalisation of the state). For a  $B$  meson at rest only  $J_{A_0}$  is relevant and the right-hand-side of the equation above becomes  $m_B f_B$ .

The way in which  $f_B$  is calculated on the lattice is illustrated in Figure 22. On the

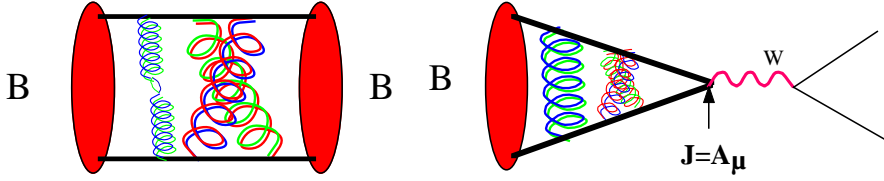


**Figure 22.** (Left) The calculation on the lattice of the 2-point correlator for a  $B$  meson. (Right) The calculation on the lattice of a 2-point function in which a  $B$  meson decays leptonically.

left-hand side is an illustration of the usual operator (correlator) whose expectation value we calculate to determine the  $B$  meson mass or energy. Then, as earlier,

$$\langle\langle H^\dagger(T)H(0) \rangle\rangle = \sum_n C_n e^{-E_n a T}. \quad (37)$$

For the  $B$  meson  $C_0$  in the fit above is equal to  $(\langle 0|H|B \rangle)^2/2E_0$ , with a relativistic normalisation of the states. On the right-hand-side of Figure 22 we illustrate the operator in which the  $B$  meson is destroyed by the axial vector current (the  $W$  decay to leptons is handled analytically and separately from the lattice QCD calculation). Then

$$\frac{1}{Z} \langle 0|H^\dagger(T)J_{A_\mu}(0)|0 \rangle = \langle\langle H^\dagger(T)J_{A_\mu}(0) \rangle\rangle = \sum_n D_n e^{-E_n a T}. \quad (38)$$

We again have a product of  $M^{-1}$  factors to average over configurations, since  $J_{A_\mu}$  contains the same kind of product of  $\bar{\psi}$  and  $\psi$  fields as  $H$ . The same energies appear in this fit (indeed the correlators should be fit simultaneously to ensure that this is true) but the amplitudes are different. Now  $D_0 = (\langle 0|H|B \rangle)(\langle B|J_{A_\mu}|0 \rangle)/2E_0$ . The second factor is the matrix element that we want and we can extract this as  $2E_0 D_0 / \sqrt{(2E_0 C_0)}$ . If the temporal axial current is used for a  $B$  meson at rest then  $f_B \sqrt{m_B} a^{3/2} = \sqrt{2/C_0} D_0$ .

The current  $J_{A_\mu}$  that we use on the lattice needs to be well-matched to the continuum current. The leading term in the lattice version of the current will be just be the obvious transcription of the continuum current,  $A_\mu = \bar{\psi}_b \gamma_\mu \gamma_5 \psi_u$ . However this current has discretisation errors at  $\mathcal{O}(\alpha_s a)$  and these can be improved by adding higher order operators to cancel the errors in the same way as for the action earlier. Again we can use perturbation theory to calculate the coefficients of these correction terms. If we use NRQCD for the  $b$  quark in the current then there are also relativistic corrections that can be applied to make the current a more accurate version of the continuum current. In fact the relativistic correction operators and the discretisation correction operators are the same and simply pick up perturbative coefficients that are functions of  $m_Q a$  (Morningstar and Shigemitsu 1998).

We also have to renormalise the matrix elements from the lattice to an appropriate continuum renormalisation scheme such as  $\overline{MS}$ . This can be done in perturbation theory as, again, it takes account of gluons with momenta above the lattice cut-off. Such calculations have only been done through  $\mathcal{O}(\alpha_s)$  so far and this means that the final quoted

result has errors at  $\mathcal{O}(\alpha_s)^2$  (Morningstar and Shigemitsu 1998). Now that the systematic error from working in the quenched approximation has been overcome, this is often the largest source of error and much more work must be done in future to reduce this error. Methods for renormalisation and matching that use direct numerical methods on the lattice (often called nonperturbative) are also being explored by many people. Matrix elements of conserved currents do not need renormalisation and this explains why, for example, the calculations of  $f_\pi$  and  $f_K$  described above are so accurate.

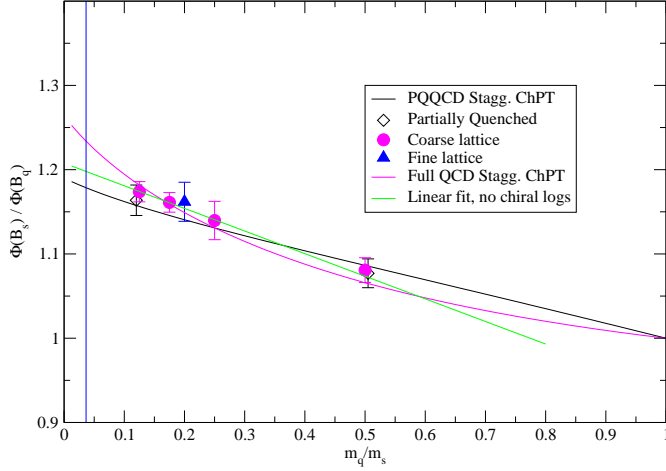


**Figure 23.** The ratio of  $f_{B_s}\sqrt{m_{B_s}}/f_B\sqrt{m_B}$  from unquenched lattice calculations on the MILC configurations at two values of the lattice spacing (Gray *et al.* 2005). The lines represent fits using chiral perturbation theory to various combinations of valence and sea light quark masses. The pink curve is the full QCD curve that extrapolates to the physical answer.

The  $B$  meson decay constant is of interest, both because it sets the rate of  $B$  leptonic decay but also because it appears in the mixing rate of neutral  $B$  mesons. The mixing rate is parameterised by  $f_B^2 B_B$  where  $B_B$  is the ‘bag constant’.  $f_B^2 B_B$  is being calculated in lattice QCD but it is harder than the calculation of  $f_B$  alone. We believe that the  $B_B$  factor is fairly benign with a value around 1. The calculation of  $f_B$  then provides a good indicator of the size of mixing effects (for the orange and yellow rings in Figure 21) until  $f_B^2 B_B$  is known accurately.

Figure 23 shows the current results by the HPQCD collaboration, using the MILC unquenched configurations and the NRQCD formalism for the valence  $b$  quarks and asqtad improved staggered formalism for the valence light quarks (Gray *et al.* 2005, Wingate 2004). What is plotted is the ratio of  $f_{B_s}\sqrt{m_{B_s}}/f_B\sqrt{m_B}$  in which the overall renormalisation constant for the lattice  $J_{A_0}$  cancels giving an accurate result. What is interesting here is the approach to the light quark mass limit in which  $m_{u/d}$  takes its physical value. Chiral perturbation theory expects fairly strong logarithmic dependence but earlier results worked at such heavy  $m_{u/d}$  that they were not in the region in which chiral perturbation theory was valid. It is clear that the new results now have light  $m_{u/d}$  and an accurate result for this ratio will be possible.

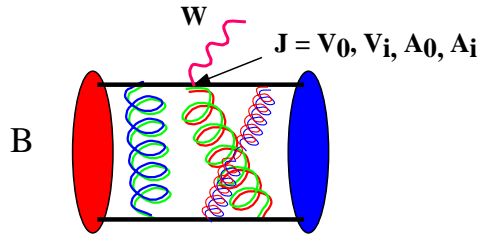


**Figure 24.** The calculation of a 3-point function for  $B \rightarrow \pi$  semileptonic decay on the lattice.

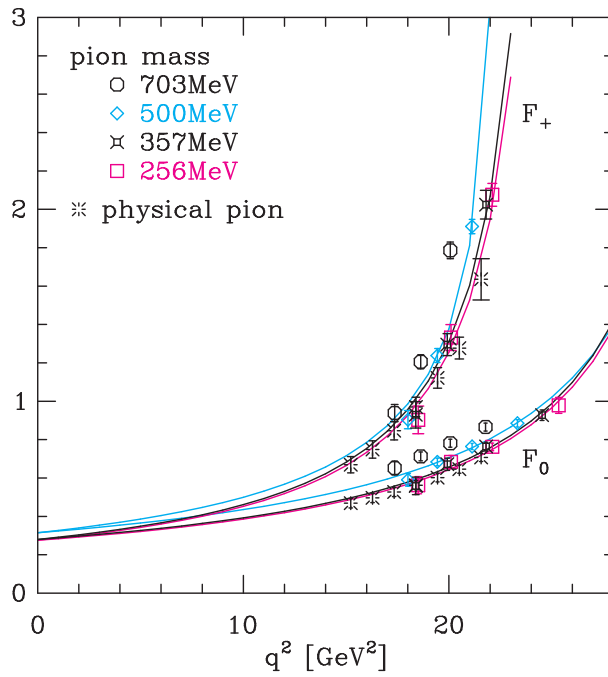


**Figure 25.** Results for the form factors for  $B \rightarrow \pi$  semileptonic decay from unquenched lattice QCD (Shigemitsu et al. 2005). Results are shown for a variety of light quarks, given in terms of the mass of the  $\pi$  made from these quarks. The bursts show the (small) extrapolation to the real  $\pi$  mass.

The determination of semileptonic decay rates requires the calculation of a 3-point function on the lattice. This is illustrated in Figure 24 for  $B \rightarrow \pi$ . We now have two hadron operators at 0 and  $T$  for different hadrons and an intermediate current operator

$J_{V_\mu}$  or  $J_{A_\mu}$  which causes the quark flavour change and the emission of a  $W$ . Now

$$\frac{1}{Z} \langle 0 | H^\dagger(T) J(t) H'(0) | 0 \rangle = \langle \langle H^\dagger(T) J(t) H'(0) \rangle \rangle = \sum_n D_n e^{-E_n a(T-t)} e^{-E' a t}. \quad (39)$$

The amplitudes,  $D_n$ , are now related to  $\langle 0 | H | B \rangle \langle B | J | \pi \rangle \langle \pi | H' | 0 \rangle$  and the matrix element that we want,  $i e \langle B | J | \pi \rangle$  can be extracted by simultaneously fitting the relevant 2-point functions to determine the other factors in  $D_0$ . The matrix element is now a function of the 4-momentum transfer between  $B$  and  $\pi$ ,  $q^2$ . It is expressed in terms of two different form factors,  $f_+(q^2)$  and  $f_0(q^2)$ , with different momentum-dependent prefactors.  $f_+(q^2)$  is the form factor that translates directly into the rate of semileptonic decay, since  $f_0$  ends up in this rate multiplied by the mass of the lepton into which the  $W$  decays, which is very small.

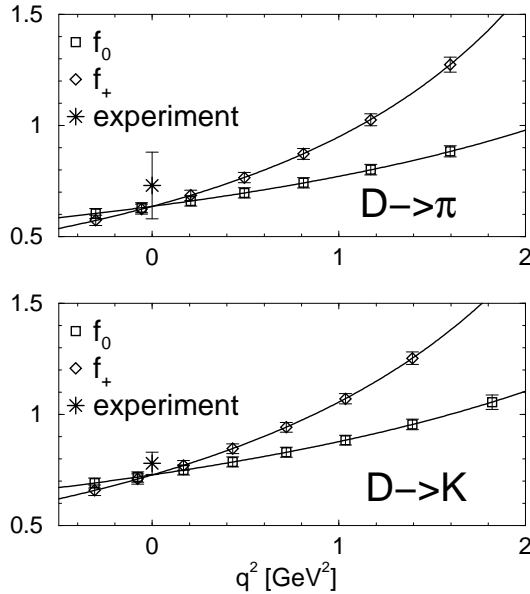


**Figure 26.** Results for the form factors for  $D$  semileptonic decay to  $\pi$  and  $K$ . The experimental points shown at  $q^2 = 0$  use the experimental decay rate at that point and the current PDG results for the appropriate CKM elements (Aubin *et al.* 2005).

Once again we must match the lattice current to a continuum current and renormalise to obtain results in a continuum renormalisation scheme. This limits the accuracy with which these calculations can now be done and more work is required to improve this situation. Figure 25 and Figure 26 show current results obtained by the HPQCD and FNAL/MILC collaborations for the formfactors for  $B \rightarrow \pi$  decay and  $D \rightarrow \pi/K$  decay respectively. The  $B$  results use NRQCD  $b$  quarks (Shigemitsu *et al.* 2005); the  $D$  results use the Fermilab formalism for the  $c$  quark (Aubin *et al.* 2005). The usefulness of the  $D$  results is to compare to imminent experimental results from the CLEO-c collaboration that will provide a check of lattice methods and systematic errors for confidence in our precision  $B$  results (Shipsey 2005).

## 4 Conclusions

Lattice QCD has come a long way from the original calculations of the 1970s. The original idea that we could solve a simple discretisation of QCD numerically by ‘brute force’ has been replaced by a more sophisticated approach. Improved discretisation of both the gluon action and the quark action has led to the possibility of performing realistic simulations of QCD on current computers. Indeed this has been done, and I hope that I have conveyed something of the excitement of seeing accurate lattice calculations reproduce well-known experimental numbers for the first time. These first calculations are of the masses of ‘gold-plated’ hadrons, those for which lattice QCD must be able to get the right answer if it is to be trusted at all. Leading on from this we have been able to make the first accurate lattice QCD prediction of the mass of a new meson, the  $B_c$ .

It is now important to beat down the sources of systematic error in the lattice calculation of decay matrix elements for  $B$  and  $D$  physics to obtain results that can be combined with experiment to give an accurate determination of elements of the CKM matrix. The timescale for this programme is the next two years and, as well as lattice QCD calculations, it requires  $\mathcal{O}(\alpha_s^2)$  calculations in perturbation theory to renormalise the lattice results to numbers appropriate to the continuous real world. On a longer timescale (say five years) studies of more complicated baryonic matrix elements will be undertaken and progress will be made in understanding to what extent accurate lattice calculations can be done of some of the more interesting, but not gold-plated, particles in the hadron spectrum.

## Acknowledgements

It was a pleasure to contribute to this interesting school. I am grateful to a large number of lattice colleagues, but particularly my long-standing collaborators Peter Lepage and Junko Shigemitsu, for numerous useful discussions over many years.

## References

There are a number of books on lattice QCD that provide more information on the theoretical background, such as Smit, 2002, *An introduction to Quantum Fields on a lattice*, Cambridge University Press. The annual lattice conference provides up-to-date review talks and access to the literature. The 2004 Conference Proceedings is published in *Nucl Phys B Proc Suppl* **140**. Below I provide a few references, concentrating on other summer school lectures where possible.

- Acosta D *et al.* [CDF collaboration], 2005, hep-ex/0505076.
- Alford M *et al.* , 1995, *Phys LettB* **361** 87, hep-lat/9507010.
- Allison I *et al.* [HPQCD/FNAL collaborations], 2005, *Phys Rev Lett* **94** 172001, hep-lat/0411027.
- Arndt D, PhD thesis, University of Washington, USA, hep-lat/0406011.
- Aubin C *et al.* [MILC collaboration], 2004a, *Phys Rev D* **70** 094505, hep-lat/0402030.

- Aubin C *et al.* [MILC collaboration], 2004b, *Phys Rev D* **70** 114501, hep-lat/0407028.  
Aubin C *et al.* [HPQCD/MILC collaborations], 2004c, *Phys Rev D* **70** 031504, hep-lat/0405022.  
Aubin C *et al.* [FNAL/MILC/HPQCD collaborations], 2005, *Phys Rev Lett* **94** 011601, hep-lat/0408306.  
Bali G, 2000, *Phys Rep* **343** 1, hep-lat/0001312.  
Bernard C [MILC collaboration], 2001, *Phys Rev D* **64** 054506, hep-lat/0104002.  
Chiu T, 2004, *Nuc Phys B Proc Suppl* **129** 135, hep-lat/0310043.  
CKMfitter, 2005, <http://ckmfitter.in2p3.fr/>  
Davies C, 1998, Springer lecture notes in physics, Eds Gausterer, Lang, hep-ph/9710394.  
Davies C *et al.* , 2005, *Nuc Phys B Proc Suppl* **140** 261, hep-lat/0409039.  
Davies C *et al.* [HPQCD/UKQCD/MILC/FNAL collaborations], 2004, *Phys Rev Lett* **92** 022001, hep-lat/0304004.  
di Pierro M, 2000, lectures given at the GSA summer school on Physics on the Frontier, hep-lat/0009001. Includes code for example calculations.  
di Pierro M *et al.* [Fermilab collaboration], 2004, *Nucl Phys B Proc Suppl* **129** 328, hep-lat/0310045; *Nucl Phys B Proc Suppl* **129** 340, hep-lat/0310042.  
El-Khadra A *et al.* , 1997, *Phys Rev D* **55** 3933, hep-lat/9604004.  
Follana E *et al.* [HPQCD/UKQCD collaborations], 2004, *Phys Rev Lett* **93** 241601, hep-lat/0406010.  
Frezzotti R, 2005, *Nuc Phys B Proc Suppl* **140** 134, hep-lat/0409138.  
Gray A *et al.* [HPQCD/UKQCD collaborations], 2003, *Nuc Phys B Proc Suppl* **119** 592; hep-lat/0507013, accepted for publication in *Phys Rev D*.  
Gray A *et al.* [HPQCD collaboration], 2005, *Nuc Phys B Proc Suppl* **140** 446; and in preparation.  
Hein J *et al.* [HPQCD/UKQCD collaborations], 2003, *Nucl Phys B Proc Suppl* **119** 317, hep-lat/0209077.
- Ishikawa K *et al.* [JLQCD/CP-PACS collaborations], 2005, *Nuc Phys B Proc Suppl* **140** 225, hep-lat/0409124.  
Lepage P, 1996, Schladming winter school, hep-lat/9607076.  
Lepage P, 1998a. For a useful discussion of path integrals in quantum mechanics and their relevance to lattice QCD see *Lattice QCD for novices*, HUGS98, hep-lat/0506036. Includes code for example calculations.  
Lepage P, 1998b, *Phys Rev D* **59** 074502, hep-lat/9809157.  
Lepage P *et al.* , 1992, *Phys Rev D* **46**, 4052, hep-lat/9205007.  
Lepage P and Mackenzie P, 1993, *Phys Rev D* **48**, 2250, hep-lat/9209022.  
Lepage P and Davies C, 2004, *Int J Mod Phys A* **19** 877.  
Mason Q *et al.* [HPQCD/UKQCD collaborations], 2005, *Phys Rev Lett* **95** 052002, hep-lat/0503005.  
Morningstar C and Shigemitsu J, 1998, *Phys Rev D* **57** 6741, hep-lat/9712016.  
Nobes M, 2005, hep-lat/0501009.  
Nobes M *et al.* , 2005, in preparation.  
Orginos K *et al.* , 1999, *Phys Rev D* **60** 054503, hep-lat/9903032.  
PDG, 2004, <http://pdg.lbl.gov/>  
Shigemitsu J *et al.* [HPQCD collaboration], 2005, *Nuc Phys B Proc Suppl* **140** 464, hep-lat/0408019.  
Shipsey I, 2005, *Nuc Phys B Proc Suppl* **140** 58, hep-lat/0411009.  
Sommer R, 1994, *Nuc Phys B* **411** 839, hep-lat/9310022.  
Toussaint D and Davies C, 2005, *Nuc Phys B Proc Suppl* **140** 234, hep-lat/0409129.  
Trottier H, 2004, *Nuc Phys B Proc Suppl* **129** 142, hep-lat/0310044.  
Wingate M [HPQCD collaboration], 2004, *Phys Rev Lett* **92** 162001, hep-lat/0311130.